General Disclaimer

One or more of the Following Statements may affect this Document

- This document has been reproduced from the best copy furnished by the organizational source. It is being released in the interest of making available as much information as possible.

- This document may contain data, which exceeds the sheet parameters. It was furnished in this condition by the organizational source and is the best copy available.

- This document may contain tone-on-tone or color graphs, charts and/or pictures, which have been reproduced in black and white.

- This document is paginated as submitted by the original source.

- Portions of this document are not fully legible due to the historical nature of some of the material. However, it is the best reproduction available from the original submission.

STUDY OF THE REMOTE MEASUREMENT OF OCEAN COLOR FINAL REPORT

Contract No. NASW- 1658

26 January 1968

Prepared for

NASA HEADQUARTERS
Washington, D.C.

STUDY OF THE REMOTE MEASUREMENT OF OCEAN COLOR FINAL REPORT

REPORTING PERIOD
28 August 1967 to 28 January 1968

Contract No. NASW-1658

26 January 1968

Prepared for
NASA HEADQUARTERS
Washington, D.C. 20546

Prepared by: Richard C Ramsey
Richard C. Ramsey
Project Manager

Approved by:
Peter G. White, Manager
Electronic Systems Department

Approved by: A. Fiul
A. Fiul, Manager
Advanced Systems Laboratory

TRW SYSTEMS GROUP

PRECEDING PAGE BLANK NOT FILMED.

CONTENTS

CONTENTS (Concluded)

ILLUSTRATIONS

ILLUSTRATIONS (Continued)

ILLUSTRATIONS (Continued)

ILLUSTRATIONS (Concluded)

TABLES

1. SUMMARY

This report contains the results of a study to evaluate the factors which affect remote measurements of ocean color and to define a set of requirements for a system to make these measurements from a spacecraft. The effects of atmosphere, sun, ocean surface, and ocean contents on these measurements are evaluated. Calculations of upward flux through the atmosphere from ocean waters containing various amounts of chlorophyll are used to define the system requirements. A preliminary design of a sensor, utilizing the WISP concept of TRW Systems, is provided with the capability of distinguishing between zero and 0.2 mg/m^3 of chlorophyll in ocean waters. This design requires the measurement of upward flux in fifteen spectral bands with a ground resolution of 2500 feet and yields total ocean coverage in 14 days from a 287 nautical mile sun-synchronous orbit.

2. INTRODUCTION

This final report is the result of a 5-month study of the remote measurement of ocean color by the application of the Wide Range Image Spectrophotometer. The study was performed for the Spacecraft Oceanography Project under NASA Contract number NASW-1658.

Richard C. Ramsey was the project manager of the study. It was performed in the Electronic Systems Department of the Advanced Systems Laboratory of TRW Systems.

The general tasks envisaged at the beginning of the program were:

- Task 1 - Analysis

  Conduct analysis of the spectral variation of the optical characteristics of the sea water as viewed from a location in or above the earth's atmosphere. This analysis was to include evaluation of the effects of surface conditions. If necessary, simple laboratory tests using TRW owned equipment would be used to evaluate the effect of surface roughness (Sections 3 through 6).

- Task 2 - Definition of System Requirements

  Based on the analysis of Task 1, a set of requirements would be prepared for a system capable of measuring the spectral characteristics of water from a moving vehicle. Both aircraft and spacecraft would be considered (Section 7).

- Task 3 - System Definition

  Based on the requirements of Task 2, a preliminary design of a system to best meet these requirements would be performed. This design would include specification of major components and a preliminary evaluation of weight, dimension, and power requirements (Section 7).

It is felt that these tasks have been completed during this study. It was not considered necessary to perform the laboratory tests of the effects of surface conditions because some previous measurement data were available in the literature and because of the difficulty in simulating real conditions.

Color, as referred to henceforth, is not that sensation as perceived by the human eye and the usual tri-stimulus method of specifying color is not considered. Instead, color is defined by describing the intensity versus

wavelength curve of the radiation under consideration. This objective method gives complete information about the radiation under consideration.

Color measurements of ocean water are presently made by use of the Forel scale and Secchi disc. The apparent color of this Secchi disc, suspended one meter below the water and viewed from above, is compared with the apparent color of each of eleven tubes containing samples of colored water which together make up the Forel scale. The eleven samples range from blue to green, with a corresponding numerical designation of 1 to 11.

This method is subjective in its approach and would be impractical to use to measure large ocean areas in a short time. The Forel scale does, however, have one advantage over any remote system of measurement — it is affected to only a minor degree by atmospheric effects.

The approach considered here will be one which measures the spectral distribution of light returned from the water to a sensor that will ultimately be located in a spacecraft. Such a sensor will be first tested in an aircraft and the design arrived at will be as compatible as possible to an aircraft platform.

The spectral intensity of radiation emerging upward from the direction of the ocean surface which is measured by a spectrophotometer on a platform in (aircraft) or above the atmosphere (spacecraft) has been influenced by many factors. Beside the energy which has been selectively backscattered from the ocean (and which it is assumed is what will be measured to obtain information about the ocean itself) the atmosphere and the ocean surface will have selectively affected the spectral content of the received radiation. It is therefore necessary to know just what these contributions are since they will vary from one particular measurement to another. If they are known, either by means of other direct-measuring instruments on the platform, or determined from ground observations, their effect can be eliminated and only that spectral information relating to the ocean itself can be retained for evaluation.

The approach, therefore, was to consider each of these effects in turn. The first was the atmosphere and its effect on the solar radiation. For the most part, the literature contains measurements and calculations

which account for the behavior of the atmosphere under all types of solar and meteorological conditions. The major task therefore in this section was the gathering of this information in a manner suitable for this study.

The next subject considered was the effect of the water surface. The effects of variations from a smooth ocean on the reflection and transmission of radiation have not been as widely covered by experimenters. Some measurements have been taken, however, and these were used to draw meaningful conclusions about the effects of water surface on the remote measurement of water color.

The factors within water which determine the spectral nature of the backscattered radiation were then considered. These included absorption and scattering by the water itself as well as the various materials found in ocean water. In particular, the determination of chlorophyll content in open ocean areas has been stressed, since it is assumed that chlorophyll content is the key to ocean productivity.

Calculations were made of the upward flux from the oceans for various amounts of chlorophyll, ranging from the clearest ocean waters (no chlorophyll) to those waters containing as much as 100 mg/m^3 of chlorophyll. The influence on the total upward flux from the water for both a very clear (Rayleigh) and a very hazy or turbid atmosphere was taken into account.

On the basis of the difference in total calculated upward flux above the atmosphere between a clear ocean water and that containing 0.2 mg/m^3 of chlorophyll, the specifications for a sensor were determined.

A preliminary design of this sensor, wherein the main components were chosen, together with the expected performance is presented.

Methods of correcting the measured data for variations in water particle content, sea surface, and atmosphere are discussed.

3. THE ATMOSPHERE

After the solar energy reaches the top of the atmosphere it is transmitted directly downward through the atmosphere, scattered, absorbed, and reflected both directly and diffusely from the surface. It enters the water where it is scattered and absorbed, and part of it reenters the atmosphere where it is again affected before it reaches the measuring instrument.

Figure 1 shows spectral irradiance data as given by Kondrat'yev[1] for various values of m, the atmospheric mass, which varies with the elevation of the sun. These curves of Figure 1 are for a pure and dry atmosphere, with attenuation due only to scattering by air molecules. Where θ is the sun's altitude, m is essentially equal to $1/\sin\theta$. The curve for m = 0, the spectral irradiance reaching the earth above the atmosphere, from the sun at its mean distance, is taken from Johnson[2], who evaluated the solar constant and published values of solar spectral irradiance. Considering the curve for m = 0 of Figure 1, the variation in the spectral data over the region of interest for this study is evident. (The spectral band of 0.3 to 0.9 micron will be considered the region of greatest interest, because these values are the practical limits of spectral response for the S-25 photo-cathode surface.)

In contrast to Figure 1, the curves of Figure 2, taken from Moon[3] show the solar irradiance at the earth's surface for a standard atmosphere which contains absorption elements and aerosol scatterers.

3.1 ATMOSPHERIC ABSORPTION

In the visible part of the spectrum (which is usually considered between about 0.4 to 0.7 micron), the atmospheric absorption of the solar energy is not a major factor in determining spectral extinction, but it cannot be ignored completely. Ozone, oxygen, and water vapor all exhibit some absorption in or near the visible spectrum.

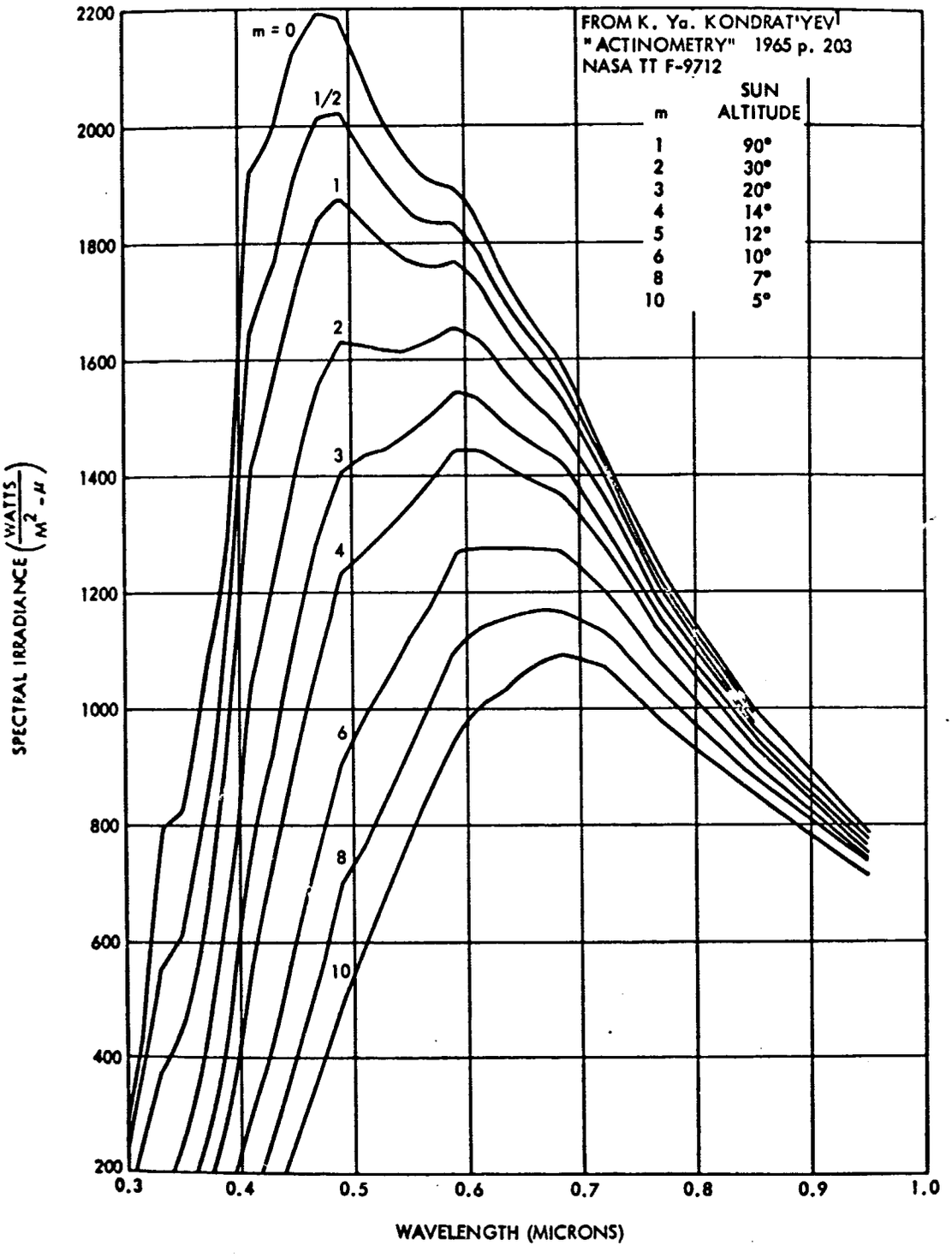

Figure 1. Solar Irradiance at Surface (Calculated for Pure and Dry Atmosphere from Molecular Scattering Theory)

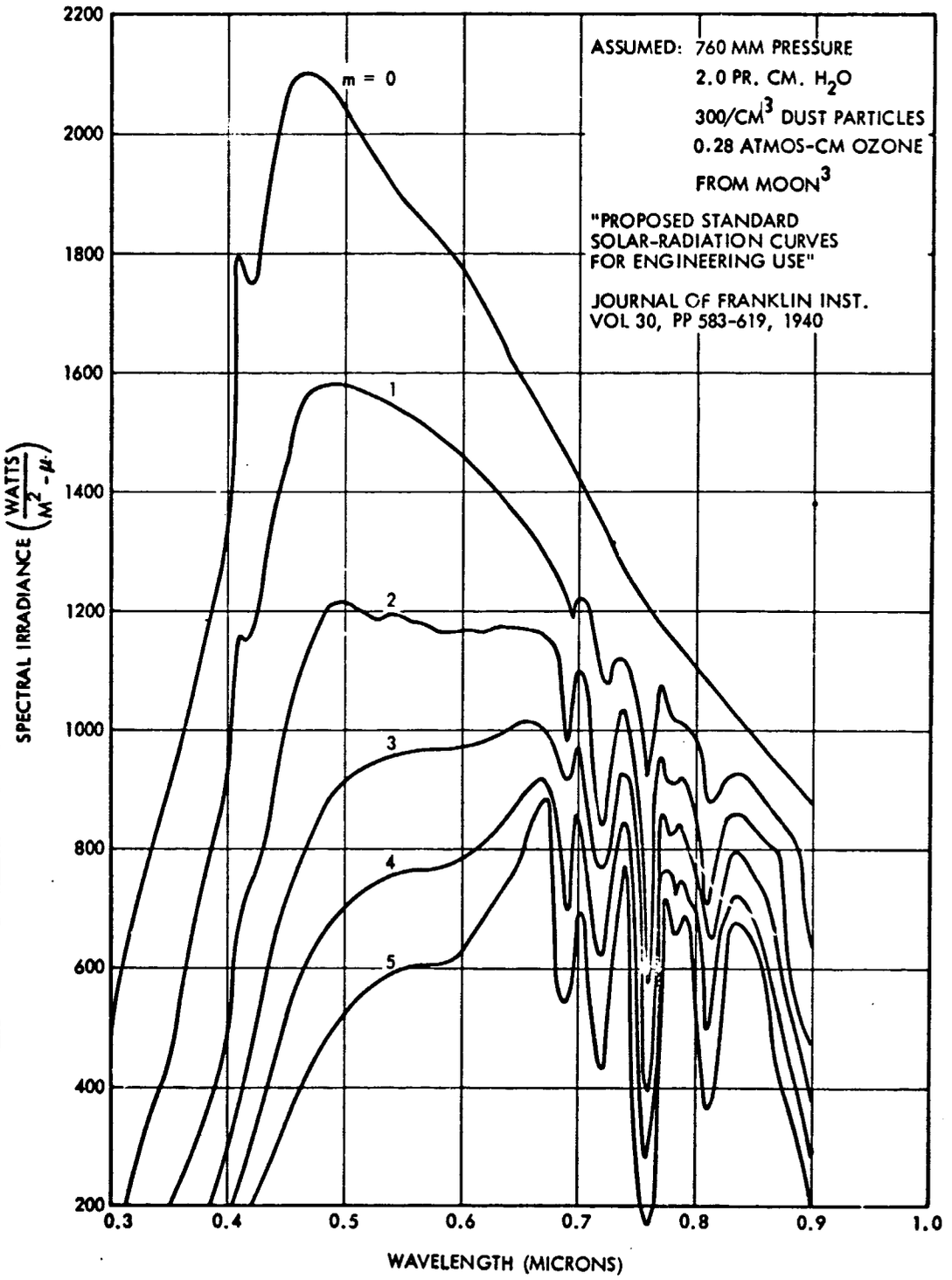

Figure 2. Solar Irradiance on Surface Normal to Sun for Standard Atmosphere Containing Absorbing and Scattering Particles

3.1.1 Ozone

Ozone plays a major role in the extinction of sunlight in the UV between 0.22 and 0.30 micron with a maximum value at 0.255 micron. In regard to the region of interest of this study (0.3 - 0.9 micron), Elterman[4] has published tables for ozone absorption by the atmosphere as a part of Standard Atmospheric Model. Figure 3 shows the variation of a representative ozone absorption coefficient β, in units of km^{-1}. For a horizontal path length, at altitude H, the transmission T_H (if extinction is considered to be only due to ozone) is

$$T_H = \exp - [\beta(H) \cdot d] \qquad (3\text{-}1)$$

where d is the path length.

The two curves represent the distribution of ozone with altitude. The amount of ozone in the atmosphere is essentially constant between 0 and 10 kilometers, increases above this to a maximum at about 23 kilometers and decreases again to where it effectively disappears at about 50 kilometers. Thus curve A of Figure 3 is representative of the absorption at about 0, 10, and 36 kilometers, with curve B showing the maximum values. Variations from this model for ozone absorption are found with season and latitude, but they are not large enough to be considered of importance.

For radiation passing upward or downward through the atmosphere, the transmission (T) can be calculated by introducing the optical density function τ where

$$T = \exp - (\tau \sec \theta) \qquad (3\text{-}2)$$

with θ the zenith angle, and

$$\tau = \sum_{0}^{H} \beta(H) \cdot \Delta H / \qquad (3\text{-}3)$$

Using the above relations, the data of Table I have been calculated to show the transmission through the atmosphere of the solar energy, for 0 and 60 degrees zenith angles, and due only to ozone extinction.

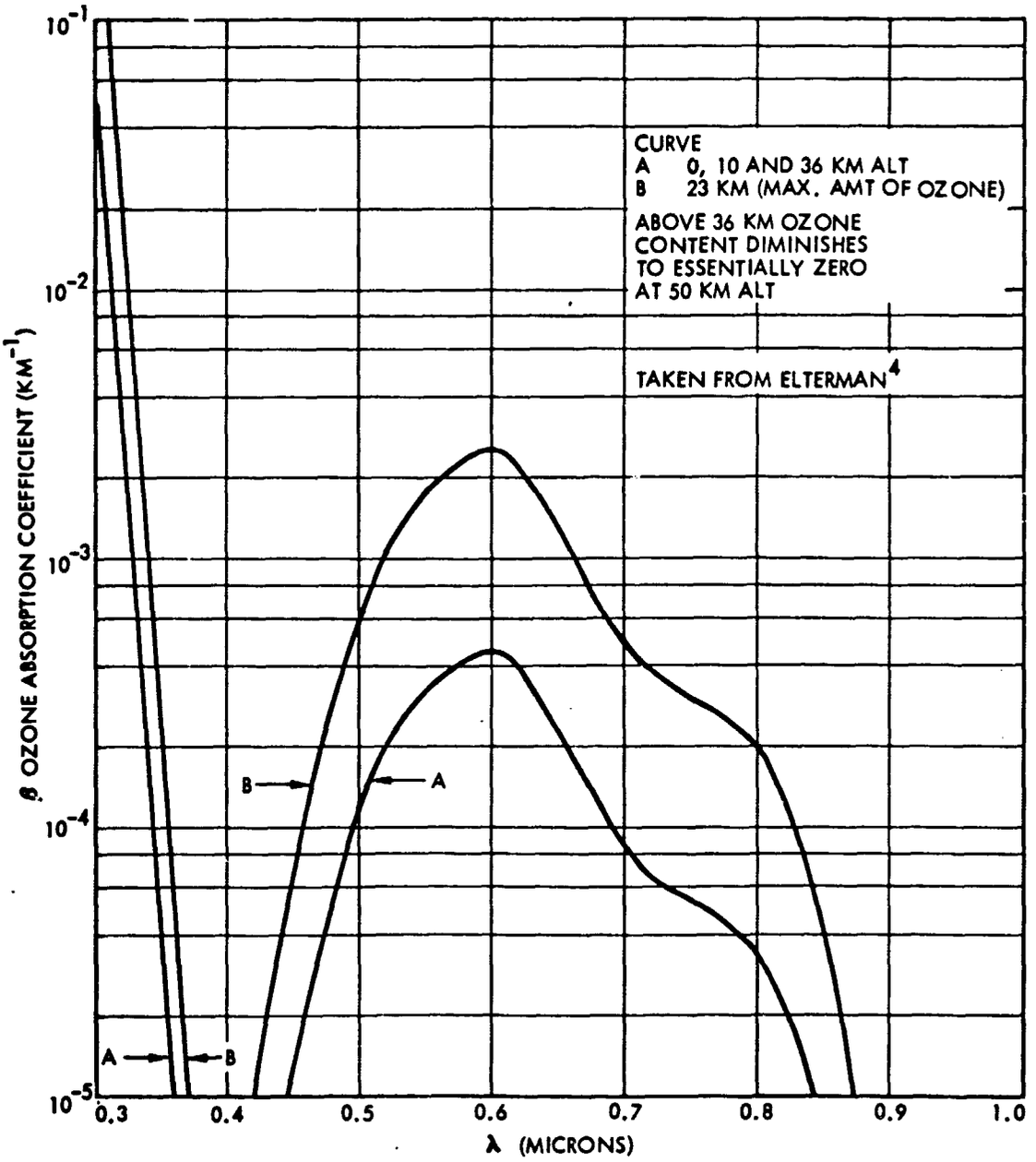

Figure 3. Spectral Absorption Coefficients for Atmospheric Ozone

Table I. Transmission of Solar Energy through Model Atmosphere (Only Ozone Extinction Considered)

Wavelength, λ (microns)	Optical Density, τ (0_3)	Transmission of Solar Energy For Two Zenith Angles, θ (percent)	
		$\theta = 0°$	$\theta = 60°$
0.3	1.39	25	6
0.4	0.000	100	100
0.5	0.011	99	98
0.6	0.045	96	91
0.7	0.009	99	98
0.8	0.003	100	99
0.9	0.000	100	100

Table I shows that variation of atmospheric transmission with wavelength, due to ozone, must be considered — although it will be seen that it is a second order effect compared to the spectral extinction due to scattering phenomena. In any event, the effect of ozone is predictable and seasonal or latitudinal variations will not essentially change the nature of the transmission data of Table I.

3.1.2 Water Vapor

Water vapor vibration-rotation bands appear in the atmosphere at 0.572, 0.592, 0.595, 0.652, 0.699, 0.723, 0.796, 0.823, and 0.930 micron with very weak bands at 0.544 and 0.505 micron (Curcio and Knestrick,[5] Kondrat'yev[6]). (Only the spectrum up to about 1.0 micron is considered here.) All of these bands up to 0.7 micron are too weak to be of any importance in this study of the effect on the solar energy spectrum. Beyond the visible and in the near infrared, there are three strong bands. They extend from 0.70 to 0.74 micron, from 0.79 to 0.84 micron and 0.86 to 0.99 micron. Kondrat'yev[1] lists a table (page 108) showing the absorption of solar radiation by water vapor in the near-infrared bands for various amounts of water vapor. It is reproduced here in part as Table II.

Table II. The Effect of Water Vapor on the Absorption of Solar Energy in Three Near IR Bands

Limits of Band (μ)	Solar Radiation at Top of Atmosphere (mW/cm^2)	Amount of Solar Radiation Absorbed (mW/cm^2)							
		H_2O content in g/cm^2							
		0.5	1.0	2.0	3.0	4.0	5.0	6.0	8.0
0.70 - 0.74	1.31	0.03	0.04	0.08	0.09	0.12	0.14	0.17	0.22
0.79 - 0.84	1.30	0.03	0.05	0.09	0.10	0.13	0.15	0.18	0.23
0.86 - 0.99	2.62	0.24	0.33	0.50	0.61	0.71	0.82	0.87	0.97

The amount of water vapor in a vertical column of the atmosphere varies from a few tenths to about 1-2 g/cm^2. The amount of water vapor in a long slant path (low sun angles) can approach some of the larger values listed in Table II. As will be seen later, no information about ocean color is available to the measuring spectrophotometer beyond 0.7 micron because of the high absorption in the sea.

3.1.3 Oxygen

There are weak oxygen bands centered at 0.698 and 0.760 micron in our region of interest, Curcio and Knestrick[5], but their effect may be considered essentially negligible for the purpose of this study.

3.2 SCATTERING – THEORY

The more important influence of the spectral nature of the radiation coming through the atmosphere is scattering. Radiation from the direct (parallel) rays of the sun is scattered, in part, on its way to the surface. After reflection from the surface, (either specular or diffuse) it is again scattered by the atmosphere. Besides primary (single particle) scattering the effect of secondary (light scattered by multiple particles) scattering must be considered in order to accurately account for the nature of the measured radiation.

Besides the extinction of radiation due to scattering (the word extinction is often used to include both the effect of attenuation due to scattering and also to absorption) there is a polarization of the scattered radiation. While the nature of the polarization of the spectral energy

that is obtained from the backscattering of the ocean water may not be pertinent to the problem in hand, the polarization of the measured component of radiation that comes from the atmosphere may provide a clue to the type of scattering occurring – and indirectly to the effect of the atmosphere on the measured ocean color.

The equations which are used to define the effects of scattering are complex, particularly for the case of multiple scattering, and it is not in the scope of this report to discuss them in detail.

The types of scattering of most importance to this study are divided into Rayleigh (or molecular), and Mie (or large particle).

3.2.1 Rayleigh Scattering

If there were no aerosol particles in the atmosphere, the spectral attenuation of radiation is easily defined by the relation of Rayleigh which states that the scattering coefficient, due to the air molecules is inversely proportional to the 4th power of the wavelength (over the range of 0.4 to 0.7 micron, the exponent is 4.08).

Rayleigh showed that the intensity of radiation is a maximum in the forward and backward direction and a minimum in the plane at right angles to the incident light.

The spectral volume scattering coefficient, $\alpha_{\varphi}(\lambda)$ is defined as the ratio of energy scattered in a unit solid angle in the direction φ to the amount incident on a scattering particle of unit volume (Kondrat'yev[1], page 159). It is given as

$$\alpha_{\varphi}(\lambda) = \frac{\pi^2(n^2-1)^2}{2N\lambda^4}(1+\cos^2\varphi) \qquad (3\text{-}4)$$

where n is the index of refraction of the scattering molecule and N is the number of particles in a unit volume.

The volume coefficient of attenuation, $\alpha(\lambda)$, is then found by summing the scattering over all angles of φ. It is given as

$$\alpha(\lambda) = \frac{8\pi^3(n^2-1)^2}{3N\lambda^4} \cdot \frac{6+3p}{6-7p} \qquad (3\text{-}5)$$

where p is the factor of polarization and equal to 0.035.

Transmission through a Rayleigh atmosphere (pure and dry air – where there is no aerosol scattering) can be easily calculated using molecular number density values from the standard atmospheric tables.

Rayleigh theory fits the measurement data when the scattering particles are smaller than the wavelength of the radiation.

Besides the air molecules, the natural aerosols found in the atmosphere are broken up into three types according to size by Junge[7]. They are given in Table III.

3.2.2 Mie Scattering

Scattering by large or giant particles cannot be accounted for by the Rayleigh theory, as discussed above. When the size of the particles becomes equivalent to the wavelength of the radiation, the λ^{-4} relationship of the attenuation coefficient no longer holds and the problem becomes quite complex when the scattering atmosphere is mainly polydisperse (composed of many different sized particles). For large particles, the intensity of scattering according to the Mie theory is predominantly in the forward direction.

The attenuation coefficient, as given by Mie is (from Middleton[7])

$$\alpha(\lambda) = N\pi a^2 K(\rho) \qquad (3\text{-}6)$$

where

a is the particle radius, and

N is the number of particles

$$\rho = \frac{2\pi a}{\lambda} \qquad (3\text{-}7)$$

Table III. Particle Sizes Found in Atmosphere, (Junge[7])

Name	Size Range (microns)
Aitken Particles	$<10^{-3} \rightarrow 10^{-1}$
Large Particles	$10^{-1} \rightarrow 10^{0}$
Giant Particles	$10^{0} \rightarrow >10^{1}$

The calculation of the function $K(\rho)$ is quite tedious and tables exist for this function for various values of the index of refraction of the assumed scattering particle.

This function $K(\rho)$ is called the scattering area ratio and is the ratio of the area of the wave front acted upon by the particle to the area of the particle itself. It varies from 0 to 4 for water droplets, with the maximum occurring near $\rho = 6.0$ (or $a/\lambda = 1$). At very large values of ρ, it tends asymptotically to the value 2, so that a large fog particle scatters twice the amount of light that would be expected from geometrical considerations.

Equation (3-6) gives the attenuation coefficient for monodisperse aerosols. In order to find the attenuation coefficient for most natural atmospheres, composed of particles of various sizes, an integration must be performed over each particle size. Thus Equation (3-7) becomes

$$\alpha(\lambda) = \sum_{i=1}^{\eta} N_i K_c(\rho) \pi a_i^2 \qquad (3\text{-}8)$$

where it is remembered that ρ is a function of λ (Equation 3-7).

Middleton[8], page 37, states that the Mie relations can be used to account for the scattering in an atmosphere when it is composed of transparent particles whose radius is between 0.1 and 2 microns. The extinction coefficient can be calculated for any aerosol if the size, number, and index of refraction is known.

To show the difficulty in predicting the variation of extinction with wavelength, Figure 4 shows values of the scattering area coefficient $K(\rho)$ in the wavelength region of interest, 0.3 to 1.0 micron, for various values of particle radii in the large particle region of haze particles (see Table III). The assumed index of refraction of the particle is 1.33, which is that of water.

If a monodisperse cloud of particles, of size equivalent to one of those used in Figure 4, is scattering light, then the spectral extinction coefficient is directly proportional to these curves. It can be seen that for small radii, values less than the wavelength, the spectral extinction

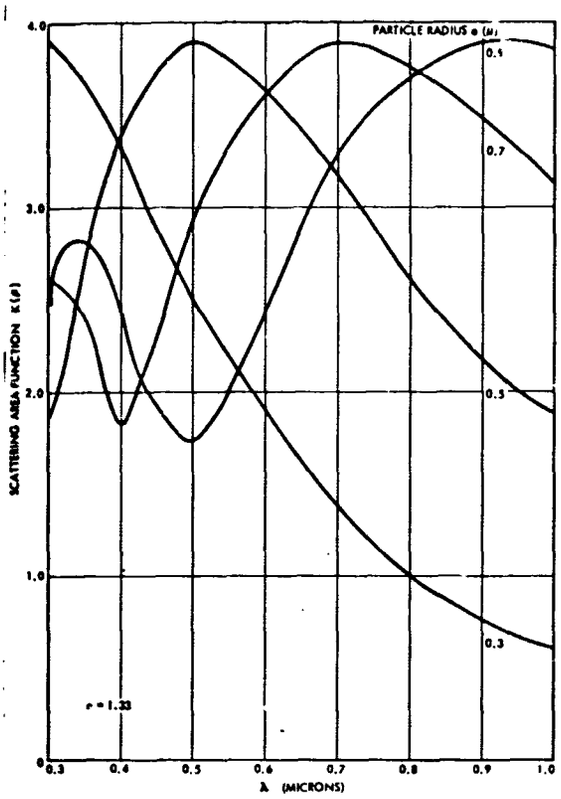

Figure 4. Scattering Area Ratio (Mie Theory) versus Wavelength for Various Particle Sizes, Middleton[8]

become proportional to $1/\lambda^n$, where finally $n \cong 4$, the Rayleigh coefficient. For large particle sizes, the value of $K(\rho)$ will approach a constant value of 2 for all wavelengths in the visible. Therefore n equals either 4 or 0 at the extremes of particle sizes, and may vary radically with wavelength for particle sizes in between.

The natural aerosol clouds are composed of particles of various radii and the difficulty of predicting the spectral extinction coefficient is obvious.

If the particle distribution (size and density) of aerosols in the atmosphere were known, then the spectral extinction could be calculated.

3.2.3 Particle Distribution

Junge[7] made measurements of the aerosol content in the atmosphere. He represented his size distribution curves in a special manner. The so-called log-radius distribution is defined by

$$n(r) = dN/d(\log r) \qquad (3-9)$$

where N is the total concentration of aerosol particles (per cm^3) from th lowest size limit up to size r. Therefore, $dN = n(r)\, d(\log r)$ is the particle number per cm^3 found between the limits of the interval d(log r Figure 5 is taken from Junge[7], and shows representative particle-size distributions.

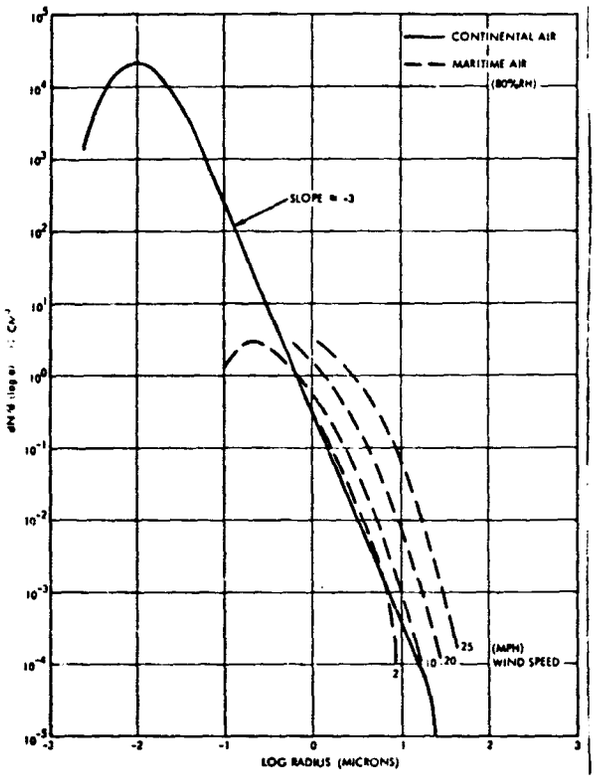

Figure 5. Average Particle Size Distribution Curve for Continental and Maritime Air Masses, Junge[7]

More data have been obtained about the continental distribution than about the maritime, especially about the variation with altitude. The data of Figure 5 correspond to low altitudes.

Since the marine atmosphere is of greater importance in this study it is of interest to consider the measurements that have been made. Roll[9] discusses the measurements made of the small Aitken and the larger particles (see Table III). Of the Aitken particles, which are found in smokes, only about 900 measurements have been made and most have been over land areas. Average density values found over the oceans are about 800 per cc; over cities, this can increase to 140,000 per cc. Of two different sets of measurements over water, a concentration of 400/cc comprised 68 percent of the observations for one and a value of 800/cc comprised 71 percent of the observations for the other. There is a large scatter in the maritime data and therefore the measurements may be influenced by continental conditions near the coast. In general, there are higher concentrations of Aitken particles in the western part of the oceans.

The large and giant particles, which predominate in maritime air, (see Figure 5), are formed by wind action at the sea surface and come from "white caps", foam, and spray. These are hydroscopic sea-salt particles. As evidenced by the distribution data of Figure 5, the radii of the sea-salt particles will vary with the relative humidity of the surrounding air. These particles are raised to higher layers by turbulence and convection until hindered by an inversion layer. Junge[7] gives data showing a marked decrease in population of sea-salt particles above about 1.5 kilometers.

Of the large particles found over the oceans, very little data have been collected. The distribution of aerosols at higher altitudes has been measured in a few cases. There is reason to believe that these high altitude distributions are not affected directly by the surface, and these measurements (made over land) will give an indication of distribution over both land and water surfaces for the troposphere and stratosphere.

Junge and Manson[10] reported some data on aerosol distributions taken from a U-2 aircraft at the 20 km level. The data showed a range of particles between 0.1 to 2μ with a pronounced upper limit in this stable layer of 20 km. The total concentration is about 0.1 per cm^3 and varies over a factor of three. The size distribution (dN/d log a) was inversely proportional to a^2. The vertical profiles showed a broad maximum between 15 and 23 km with little yearly variation.

Elterman[4] used the data of Junge and Manson[10], discussed above, plus all the previous data obtained up to altitudes of 5 km, to arrive at a representation profile of aerosol number density. This curve is given as Figure 6.

Kondrat'yev, et al[11] reports on balloon flights in the stratosphere to measure the direct solar radiation, up to 32 km, in spectral bands between 0.35 to 13μ. Extinction by aerosols was noted both above and below the tropopause ($\approx$10 km), and the attenuation tended to be stratified into various levels, such as 2 to 4 km, 6 to 10 km, 12 to 17 km, 19 to 22 km, and 23 to 25 km. In general, at the higher altitudes (above about 8 to 10 km), the aerosol attenuation showed the same relative effect with altitude as would be obtained with the assumed model atmosphere of Elterman[4], but had one to two orders of magnitude greater attenuation than that assumed by Elterman[4].

Finally, some measurements by Lloyd, et al[12] indicate what type of attenuation can be expected for the highest parts of the atmosphere. He used a rocket-borne spectrometer and made spectral measurements of the zenith sky over various sun-zenith angles and azimuth angles from the sun, from altitudes of 20 to 90 km. He concludes that above 20 km, the attenuation is Rayleigh.

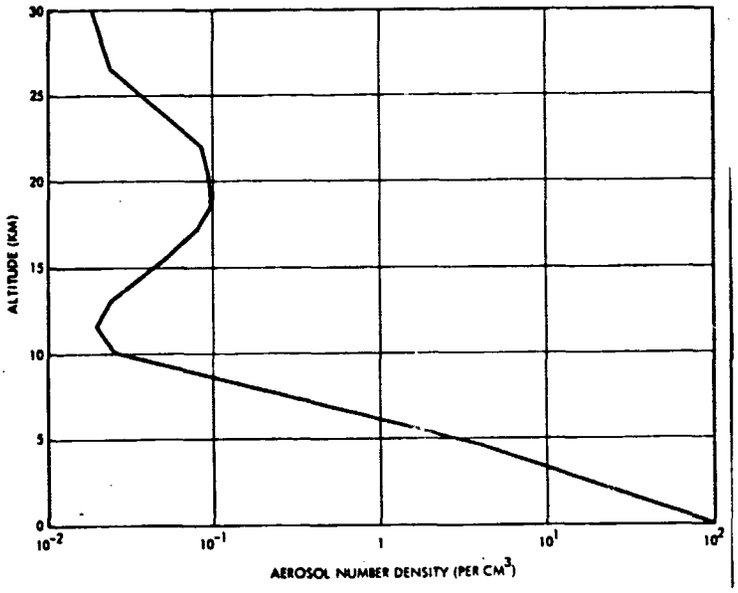

Figure 6. Representative Profile of Aerosol Number Density versus Altitude, Elterman[4]

3.4 EMPIRICAL RELATION FOR SPECTRAL ATTENUATION BY AEROSOLS

If the attenuation were only Rayleigh (molecular) in the atmosphere, then an exponent of -4 for the wavelength would adequately describe the spectral attenuation. Because most natural aerosols are polydisperse, the Mie theory must be used to explain the type of spectral attenuation expected.

Middleton[8] discusses whether an empirical relationship can be found between the extinction coefficient, σ, and the wavelength. The scattering coefficient is assumed to equal to σ if there is no absorption. If we would write

$$\sigma \sim \lambda^{n} \tag{3-10}$$

and could measure σ in a few spectral bands, then n would be known. The Mie theory gives values of n (for water droplets) in the following manner:

with small particles; $n = -4$.

when particle radius a $\begin{cases} = 1/2\ \lambda; & n = -2. \\ = 3/4\ \lambda; & n = -1. \\ = \lambda; & n = 0. \end{cases}$

Therefore, Middleton concludes that when the atmosphere is mainly polydisperse (composed of many different sized particles) it is difficult to assign a value of n. He suggests, however, that there may well be a relationship between σ and its variation with wavelength for monodisperse aerosols, and the spectral nature of transmitted light will yield the particle size. Middleton[8] also states that in fogs the visual range (distance at which target is just discernible from its background) cannot be taken as an indication of whether there is selection or nonselective scattering.

Middleton[8] summarizes the various investigations on natural haze up to 1947. He suggests that a value of n = -1.3 is representative of most of the data to that time. Further, he suggests that -1.3 corresponds to a visual range of about 30 km, and that the value of n should increase to the Rayleigh value of -4 as the visual range increases above this value. One measurement gives a value of -2.09 for a visual range of 150 km. Other data indicated a value of -1.6 for 90 km visual range. Finally, for large attenuation in fogs, where the visual range is small and consequently the value of n is expected to decrease toward zero, he reports the following empirical relationship for visual ranges (V) less than 5 km.

$$|n| = 0.0585V^{1/3} \text{ (V in meters)} \qquad (3\text{-}11)$$

Some more recent measurements tend to confirm the above empirical relationships. Curcio and Durbin[13] showed by curve fitting observational data, using the Junge particle size distribution for continental air as in Figure 5, that n equals -1.3 ±0.6 for visual ranges between 2.7 and 120 km.

Curcio, et al.[14] continued calculations and found that their measurements, taken along the coast line and over Chesapeake Bay, were best represented by assuming a two-component, composite distribution. The two components are the continental and maritime distributions of Figure 5. In addition the maritime air distribution was relatively monodisperse and contained in a narrow radius interval, (1 to 20μ).

Figure 7 is a composite of some of the theoretically-fitted curves to the experimental data, showing the variation in the spectral extinction for various measurements and how, by trial and error, a particle distribution of both continental and maritime aerosols was found. Table IV gives the details of each curve. Curves A and B show the theoretical spectral attenuation for continental (small particles) and maritime (large particle) distribution. It is of interest to note that a pure maritime aerosol in the atmosphere will show a nonselective attenuation in the region of interest, (0.3 to 1.0μ).

Table IV. Explanation of the Theoretical Curves*

Curve	Explanation	Theoretical	Visual Range (km)	Continental Distribution Data Used				Maritime Distribution Data Used			Other
				#/cc	Δλ(μ)	n	m	#/cc	Δλ(μ)	m	
A		X	——	4050	0.1-20	-3.25	1.33	——	——	——	
B		X	——	——	——	——	——	0.23	1-20	M_1-1.50 M_2-1.33	
C	X	X	4	3800	0.1-20	-3.2	1.33	3.6	1-20	1.33	90% RH 18° C
D (Either Distribution)	X	X	25	215 325	0.1-20 0.1-20	-2.8 -2.9	1.50 1.33	0.9 0.95	1-20 1-20	1.50 1.33	55% RH 20° C
E	X	X	75	120	0.1-20	-3.0	1.33	0.25	1-20	1.33	11,000 feet altitude Hawaii 5° C, 75% RH

*Used to fit Experiment Data of Figure 7

(n is exp. of radius $\frac{dN}{d \log r} - R^n$, m is index of refraction)

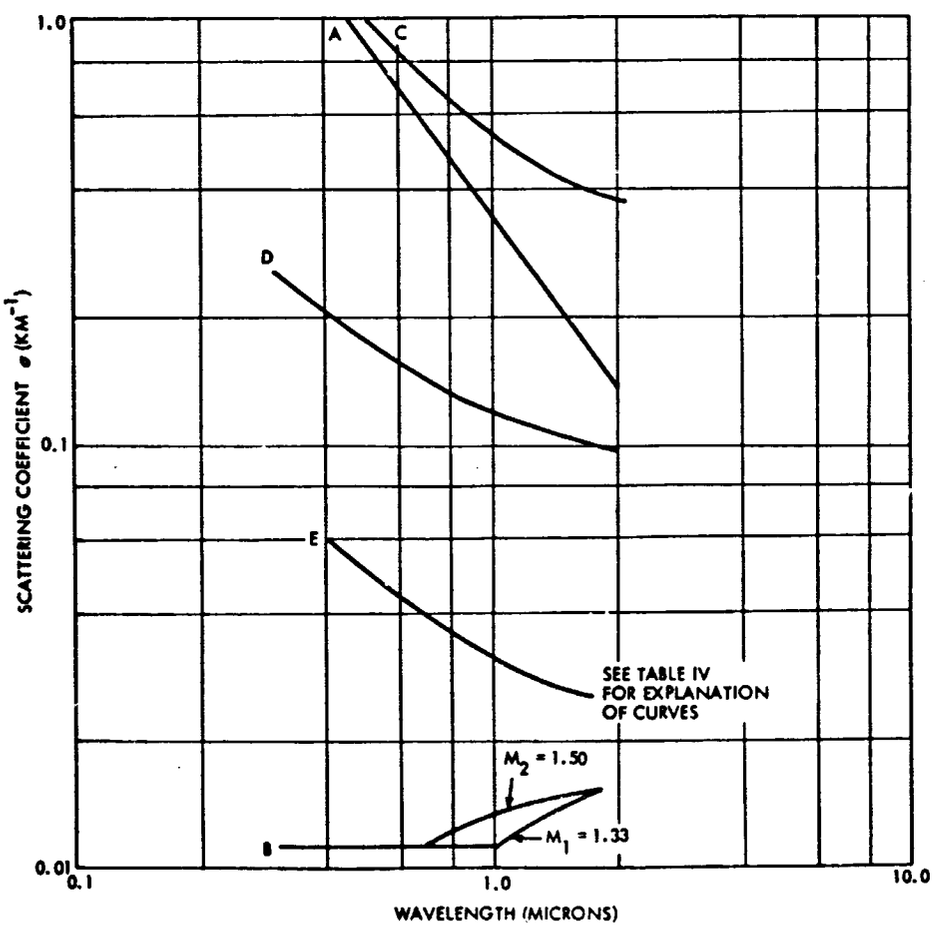

Figure 7. Experimental Attenuation of Visible and IR Radiation as Fitted by Assumed Combinations of Continental and Maritime Air, Curcio and Durbin[11]

3.5 CORRECTING FOR THE ATMOSPHERE WHEN MEASURING OCEAN COLOR

3.5.1 General Problems

The previous discussion indicated the many problems involved in the prediction of the effect of the atmosphere on the spectral extinction of radiation. For very high visibilities, the attenuation is molecular, follows the λ^{-4} relationship of Rayleigh, and therefore the atmospheric effects are easily calculable. The introduction of an aerosol in the atmosphere, with its distribution of various sizes, results in spectral extinction that is difficult to determine.

More measurements have been made over continents than over oceans, but it appears that the aerosol elements to be found, especially over water areas far from land, are sea-salt particles with a relatively simple distribution. This distribution, which consists of particles between one and two microns radius (essentially a monodisperse distribution), will tend to exhibit nonselective extinction in the visible portion of the spectrum.

The extinction experienced over coastal waters is more complex. As was shown above, a combination of both continental and maritime aerosol distributions was needed to fit the measured extinction data.

The problem arises, then, in determining a way to adjust the ocean color measurements to account for any selective extinction and scattering of the atmosphere.

Can independent measurements be made of the aerosol itself to make these adjustments? Two types of measurements suggest themselves. One is a measurement of the visible extinction of the atmosphere and the other involves measurements of the polarization of the scattered solar radiation.

3.5.2 An Independent Measurement of Extinction

One method of determining the extinction coefficient of the atmosphere, (or the visual, or meteorological, range as it is sometimes

called), is due to the theory of Koschmieder, as discussed by Middleton[8]. In its simplest form, it is

$$\frac{B_T}{B_H} = 1 - e^{-\sigma R} \tag{3-12}$$

where B_T and B_H are the radiances of a black target and the horizon, respectively. The attenuation coefficient over a path along the range, R, can be determined if these two radiances are measured. Middleton[8] also gives a more complicated form of this equation where an observer is looking downward through the atmosphere. It is

$$B_R = B_H \left[1 - e^{-\sigma \bar{R}}\right] + B_{oe}{}^{-\sigma \bar{R}} \tag{3-13}$$

where

B_R is the apparent luminance of an object when seen from a distance R

B_o is the intrinsic luminance of the object

B_H is the luminance of horizon sky

$\bar{R}$ is the optical slant range, representing the horizontal distance in a homogeneous atmosphere for which the attenuation is the same as that actually encountered along the short path R.

Now B_r and B_H can be measured, assuming a target can be found such as the sea surface over long slant ranges or a cloud. The sea surface might approach a target with zero reflectivity (zero luminance), or a cloud (if large enough to fill the field of view of the measuring instrument) could be assumed to have a reflectivity of one. Duntley[16] discusses a method of estimating the value of $\bar{R}$, the optical slant range, by assuming a simple variation with altitude of the number of scattering particles. Assuming a value of N_o for the number of particles at sea level, the number of particles at altitude y, was

$$N = N_o e^{-y/21,700} \tag{3-14}$$

which leads to the relation for the optical slant range $\bar{R}$, as a function of the actual slant range, R, and angle θ,

$$\bar{R} = 21,700 \csc \theta \left[1 - e^{-R \sin \theta / 21,700}\right] \qquad (3\text{-}15)$$

This relationship is for a rather idealized atmosphere and a different variation with height should be used to represent the particle distribution with height. Duntley[16] shows nomographs for obtaining $\bar{R}$ for various distribution and for particle stratification, which is the case for the oceans more than for the land masses. Figure 8 shows some data taken from Roll[9] showing this stratification.

With these data, the following relationship for $\bar{R}$ was found for maritime air:

$$\bar{R} = 5000 \csc \theta \left[1 - e^{-R \sin \theta / 500}\right] \qquad (3\text{-}16)$$

This holds for altitudes up to 5000 feet. Above that the sea-salt particle count can be assumed to equal zero.

3.5.3 Polarization Measurements

It has long been known that measurements, looking upward into the atmosphere, of the degree of polarization of the scattered sunlight showed that there were directions where the polarization is a maximum and in other directions no polarization was found (neutral points).

Rao and Sekera[17] discuss calculations made of the character of the radiation emerging from the atmosphere and suggests that the features of polarization are as shown in Figure 9. The diagram, in the plane defined by the sun, observer, and the nadir, purports to show the relative directions of the positions of maximum polarization and the neutral points, or no polarization.

The region of maximum polarization is about 90 degrees from the antisolar point, depending on the degree of diffuse reflectivity of the ground. The Brewster and Arago neutral points are mutually exclusive and which one appears depends on the solar elevation. The amount and vertical distribution of the atmospheric aerosol will effect the intensity and direction of these polarization parameters. Sekera[18] has solved the

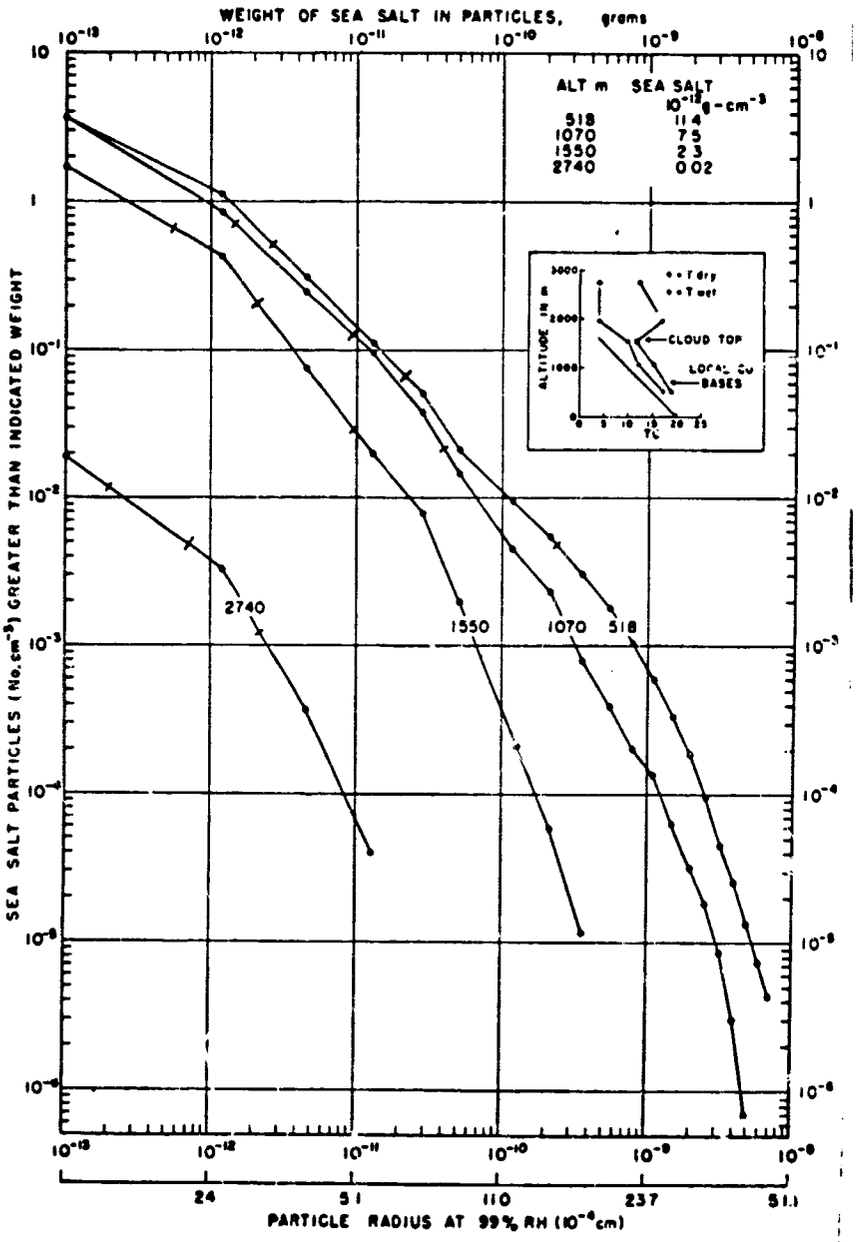

Figure 8. Size Distribution of Sea-Salt Nuclei at Different Altitudes over the Sea Near Hawaii, Roll[9]

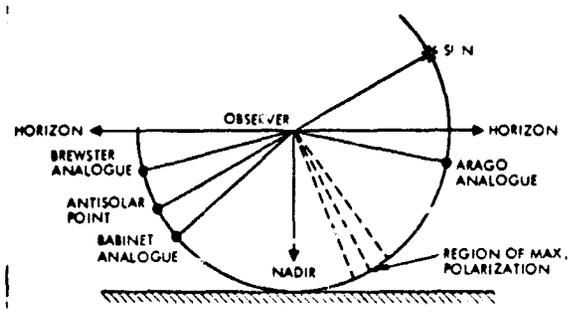

Figure 9. Polarization Features of Upward Radiation in the Principal Plane of the Sun

equations which define these parameters and gives the relationship between the optical thickness of the atmosphere and the neutral points as well as the degree of polarization in the nadir.

The theory of these effects is extremely complex and will not be given here. Many of the assumptions on which they are based, however, indicate that much experimental data need be obtained before the usefulness of the theory can be shown. The assumptions as to the type and degree of reflectivity of the surface (Lambertian or Fresnel) strongly affect the polarization parameters. Also the degree of turbidity is an important factor. High atmospheric turbidity will diminish the accuracy of the theory.

The atmosphere over the oceans (although not necessarily in coastal regions) will be marked by aerosol distributions in lower layers of relatively monodisperse sizes. Also, at least for a relatively quiet sea, the reflective properties should be well known. Therefore, an attempt to correlate ocean color measurements with polarization measurements does seem attractive in finding a method of taking into account the effects of the atmospheric scattering. Sekera, et al[19] describes a polarimeter, of a type used on balloon flights that might be used to make measurements simultaneously with the spectrophometric measurements of ocean color. He uses a rotating half-wave plate, an analyzing Glan prism, a filter wheel, and photomultiplier to measure the degree of linear polarization and relative intensity variations in four narrow spectral intervals in or near the visible. It scans in a predetermined plane. It would appear that empirical relationship between data taken with a device of this type from an aircraft and atmospheric aerosol distribution over the ocean would provide useful information for correlating ocean color raw data.

4. THE WATER SURFACE

Upwelling natural light from the sea during daylight originates from scattering from within the sea, reflection from the sea surface, and reflection from the sea bottom if the water is shallow. The spectra of upwelling light will depend on many factors, one of which is the ocean surface condition. The backscattered light is nearly independent of the presence of waves; this is not true, however, for the radiation reflected from the surface of the sea. The surface reflected light is composed of two distinct types of radiation: 1) the specularly reflected sun's rays, and 2) the diffuse skylight reflected at the sea's surface. The reflections of the highest intensity arise from small surface areas that are tilted by wave action to the angle which specularly reflects the image of the sun directly into the field of view of the sensor. These reflections are seen in highest concentration in the glitter pattern surrounding the direct reflection of the sun. The concentration decreases with increasing distance from the center of the glitter pattern, the rate of decrease depending on the sea state of the water surface.

The intensity of upwelling due to the sun's glitter on the sea surface can be determined from the distribution of wave slopes of the surface, which depends on the wind speed, and the reflection coefficient, which in turn depends on the angle of incidence and the spectral region of interest. The brightness due to direct reflected sunlight is several orders of magnitude greater than scattered radiation; therefore, spectral information from sunlight scattered from particles beneath the sea surface cannot be obtained while the sun's glitter on the sea surface is within the sensor's field of view. If a sensor is pointing in a direction around the nadir, measurements when the solar zenith is small (< 30 degrees) are undesirable.

The reflected skylight for a particular field of view of the ocean is proportional to the intensity of the skylight from the appropriate portion of the sky. The skylight intensity varies over the sky and is somewhat a function of the solar altitude. For a sensor viewing around the nadir, only the zenith skylight is of importance.

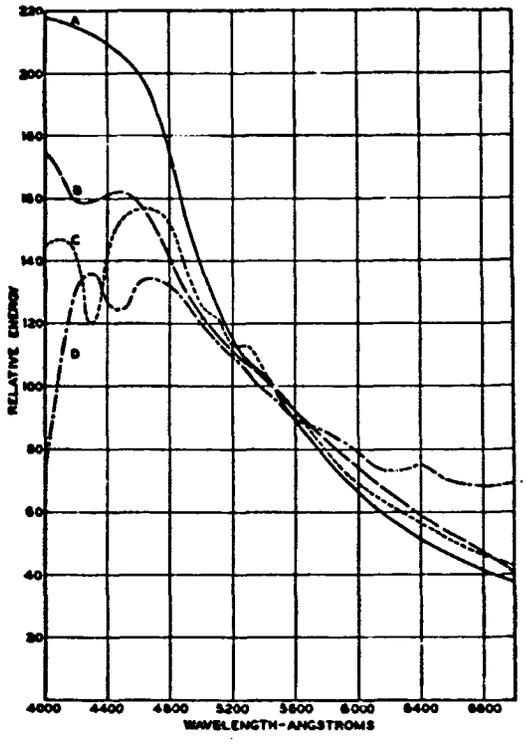

Figure 10. Spectral Distribution of Energy from the Zenith Sky a) Very Clear Sky b) Sky Hazy and Smoky (p.m.) c) Sky Clear but Smoky d) Sky Hazy and Smoky (a.m.), Taylor and Kerr[20]

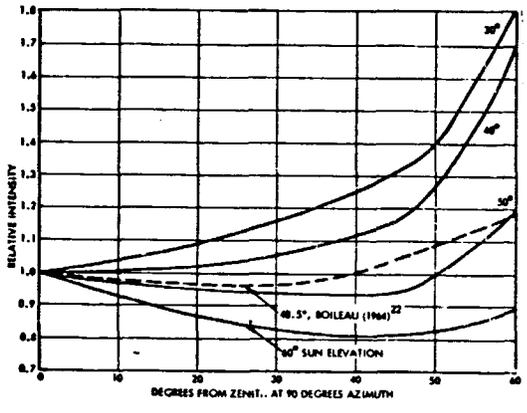

Figure 11. Measurements of Skylight at 90° Azimuth to Sun for Various Sun Elevations, Dorno[21](1919)

The spectral distribution of the skylight at the zenith is shown in Figure 10 (from Taylor and Kerr[20]). It shows the variation in the spectral content of the zenith skylight as the turbidity of the atmosphere increases from the clear condition (Rayleigh) to the hazy and smoky atmosphere, wherein the curves show the long wavelength energy becoming of more importance.

The variation in skylight luminance for different sun angles at increasing angles from the zenith is depicted in Figure 11, as taken from Dorno[21] and Boileau[22]. The data are drawn for only the 90 degree azimuth case, since the skylight gradient is generally the greatest along the azimuth direction.

An idea about the ratio of reflected sunlight to that back-scattered from beneath the water can be obtained by a consideration of various measurements of radiation from the sea.

4.1 MEASUREMENTS OF RADIATION FROM THE OCEAN

The radiation from the oceans has been measured by a number of experimenters. One of the earliest from which some information pertinent to this study can be derived is that of Powell and Clarke[23]. Photometers were stationed on a platform about 6 meters above the water and directed downward. Two wavelength regions were inspected, the violet, between

0.31μ and 0.45μ, and the red, between 0.60μ and 0.70μ. The upward irradiance was compared to the total irradiance reaching the surface from above. Some typical data are shown in Table V.

Table V. Percent of Incident Light Directed Upward from Ocean*

Sky	Wind	Sun Altitude (degrees)	Percent of Incident Light Directed Upward	
			Violet	Red
Clear	None to Light	40 — 70	4.5	2.5
Clear	8 — 18 knots	35 — 40	7.0	5.0
Overcast	None to Light	53 — 70	6.4	—

*Measured at 6 meters altitude, from Powell and Clarke[23].

Two observations are of importance in regard to these data. The first is that the higher wind speed increases the amount of bubbles at the surface and the reflectivity of the surface is increased. Second, when the sky is cloudy, the upward radiation is increased.

Cox and Munk[24] made measurements from an aircraft of the sun glitter from the water and determined the background radiation from the reflected skylight and backscattered radiation from the water. They state that these two components are of roughly equal intensity on calm days.

In addition, they indicate that this backscattered radiation from particles beneath the surface is independent of the presence of waves. Near the horizontal specular point, (that angle of viewing the ocean where a mirror-like reflection of the sun would be seen), the ratio of directly reflected radiation to that from the background (reflection skylight and backscatter from the water) is 500:1 for a smooth sea and 15:1 for a very rough sea.

Figure 12 shows their data of the ocean radiance, for both a smooth and rough sea, of the reflected, diffuse sky light as a function of the angle of viewing the ocean, δ. When δ is 0, the viewing angle is the nadir. In addition Figure 12 indicates that for viewing angles up to about 30 degrees from the vertical, the intensity of the reflected skylight is independent of the state of the sea.

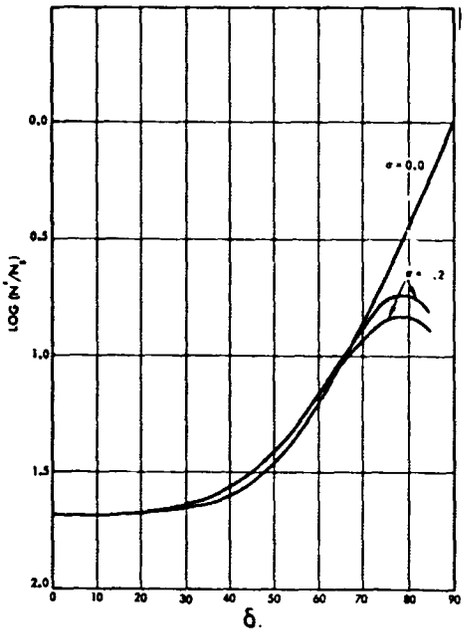

Figure 12. The Ratio of Reflected Sunlight, N', to Incident Sunlight, N_s, at Various Viewing Angles, μ, for Smooth (σ = 0.0), and Rough (σ = 0.2) Seas, Cox and Munk[24]

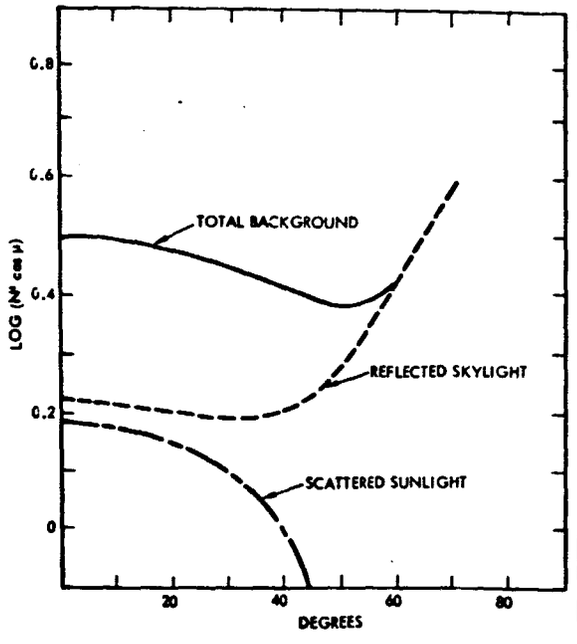

Figure 13. Measured Radiance (Outside Glitter Pattern) from Ocean on Very Calm Day and Portions Due to Reflected Skylight (Calculated) and Backscattered Sunlight from Water (Taken as Difference Between Other Two Curves), Cox and Munk[24]

Figures 13 and 14 show experimental data of the reflected and backscattered sunlight for a calm and rough ocean, respectively. The increase in reflected skylight with rough sea is shown. Thus in measuring ocean color the background, due to reflected skylight, will increase with a rough sea, while the magnitude of the backscattered radiation will drop slightly. Roll[9], as shown in Figure 15, gives a relation between sea surface and wind velocity.

Stamm and Langel[25] measured radiation from the sea from an aircraft platform at altitudes up to 2000 feet. Various atmospheric, solar, and sea conditions prevailed during the measurements. These data are presented in Figures 16, 17, 18, and 19 and show the absolute spectral intensity of the radiation from the sea. A narrow spectral bandwidth was used resulting in resolution of absorption lines in the solar spectrum, but in the data reduction smooth curves were drawn through the data so that these lines are not shown.

Figure 19 shows data for three curves (and compares them to Hulburt's[28] calculations*) taken for a range of sky conditions, but all for shallow water. There is about a 50 percent increase in intensity in

*These calculations are discussed in the next section.

going from an overcast to a clear sky. The irradiance is lower by a factor of three at 0.750μ compared to that at 0.450μ.

In Figure 19, the curves for very deep water climb almost linearly from the yellow into the blue, with a maximum spectral irradiance of 200 w $M^{-2}\,\mu^{-1}$.

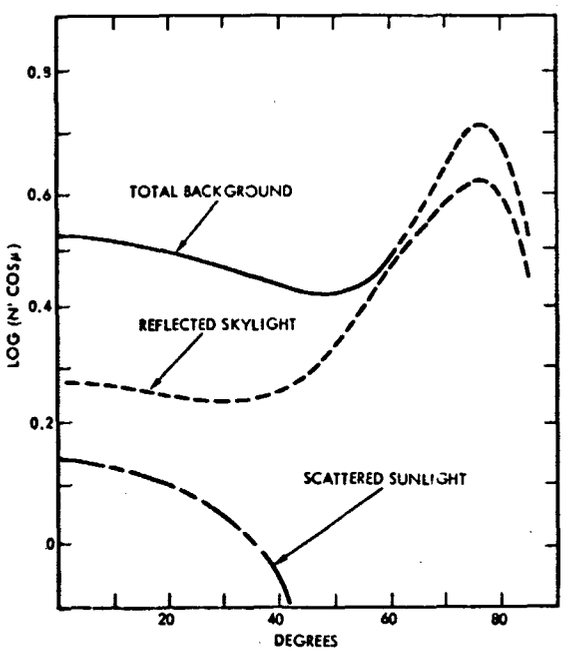

Figure 14. Measured Radiance (Outside Glitter Pattern) from Ocean on Moderately Rough Day and Portions Due to Reflected Skylight (Calculated) and Backscattered Sunlight from Water (Taken as Difference Between Other Two Curves), Cox and Munk[24]

Figure 18 shows the humping of the green, at about 0.55μ and a dip below 0.49μ — due apparently to reflection from the bottom. In Figure 19, a large hump appears on the shallow water curves, extending between about 0.43μ to 0.63μ, and when the water becomes deep, the hump disappears.

Stamm and Langel[25] make the following pertinent observations about their data:

- There is no significant change in the visible spectrum of the radiation from the sea due to changes of sky conditions, except for a change in the total irradiance.

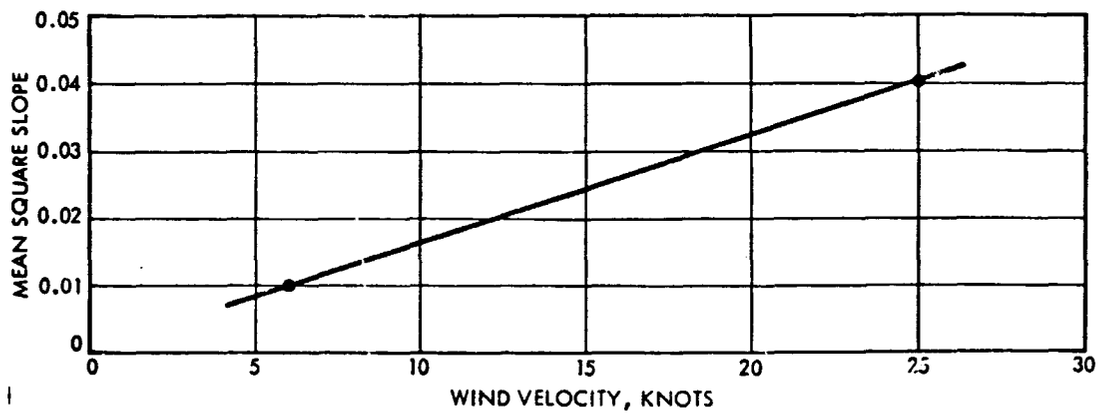

Figure 15. Sea Surface Slope Versus Wind Velocity, Roll[9]

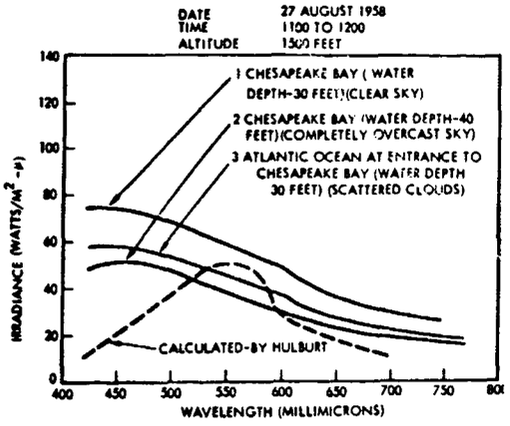

Figure 16. Typical Absolute Spectral-Irradiance Curves of Upwelling Light Over the Chesapeake Bay and the Atlantic Ocean at the Entrance to the Bay, Stamm and Langel[25]

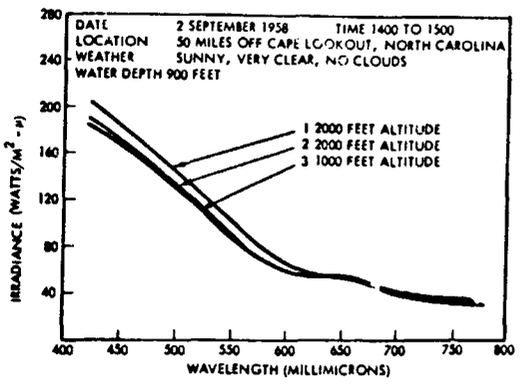

Figure 17. Typical Absolute Spectral-Irradiance Curves of Upwelling Light over the North Atlantic Ocean Approximately 50 Miles off Cape Lookout, North Carolina, Stamm and Langel[25]

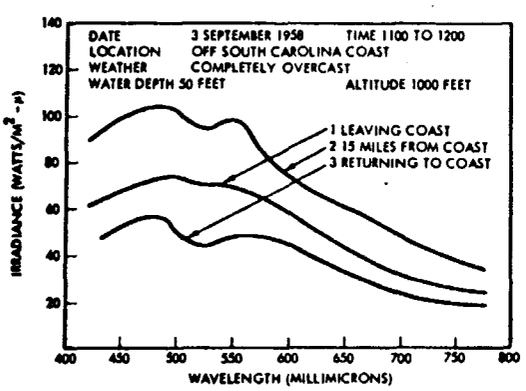

Figure 18. Typical Absolute Spectral-Irradiance Curves of Upwelling Light over the North Atlantic Ocean Approximately 15 Miles off the South Carolina Coast between Charleston, South Carolina and Savannah, Georgia, Stamm and Langel[25]

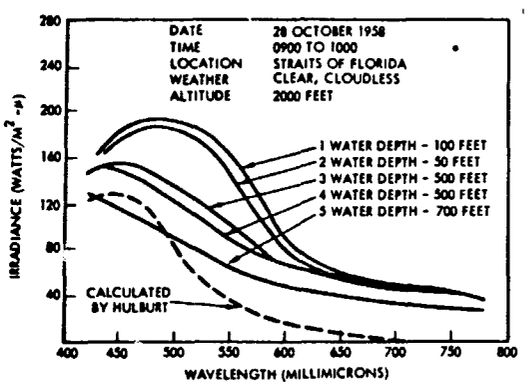

Figure 19. Typical Absolute Spectral-Irradiance Curves of Upwelling Light over the Straits of Florida, Stamm and Langel[25]

- Bottom reflectances affect the color of the sea markedly by enhancement of the green.
- The differences in the spectra obtained all occur between 0.42μ and 0.60μ.
- The surface reflection contributes a major portion of the measured radiation in the red portion of the spectrum. (This conclusion was made by comparing the measured curves of Figure 16 with the calculated data of Hulburt[28], which omitted the contribution from surface reflection.)
- At higher altitudes the measured radiance is affected more by atmospheric scattering.

This last observation is confirmed quite strongly by the measurements of Duntley[26]. He measured the upward irradiance from the sea by use of a

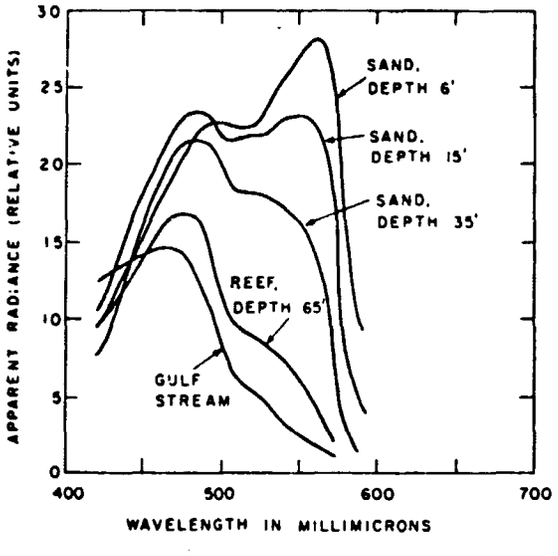

Figure 20. Spectroradiometric Curves of Light from the Nadir Reaching a Spectrograph Mounted in a Glass-Bottomed Boat over Shoal off Dania, Florida (March 1944). Spectral resolution: 7.7 mμ; Spatial Resolution: 2.0×10^{-6} sr, Duntley[26]

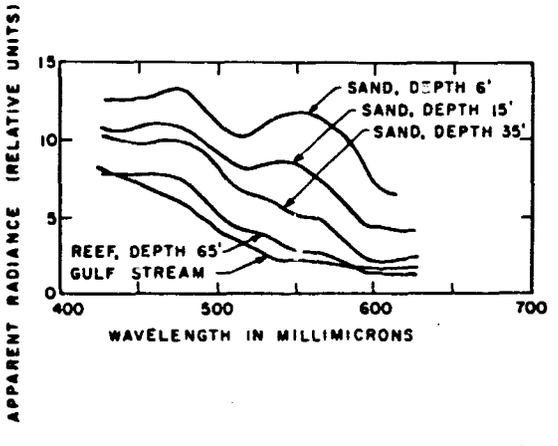

Figure 21. Spectroradiometric Curves of Light from the Nadir Reaching a Spectrograph in an Airplane 4300 Feet Above the Same Ocean Locations as in Figure 20. Spectral Resolution: 7.0 mμ, Spatial Resolution: 3.2×10^{-6} sr, Duntley[26]

spectrograph (pointing to the nadir) located in a glass bottomed boat. Figure 20 shows the strong blue color for the deep water and the color of sand predominating in shallow water. The aircraft data shown in Figure 21, and taken from the nadir at 4300 feet, over the same water shows the same effect, but the atmospheric scattering and the surface reflection tends to make these differences. The spectral resolution was about 70 Å for these measurements.

4.2 SOME PREVIOUS CALCULATIONS

Hulburt[27] derived equations in order to explain the radiation flowing upward and downward in an absorbing and scattering medium, with both collimated and diffuse radiation incident on the upper surface. He assumed the boundaries of the medium are infinite in horizontal directions. These equations were used[28] to calculate the spectral intensity of upcoming radiation, with an overcast sky and deep water, for the waters of the coastal Gulf Stream, Chesapeake Bay, and for distilled water. Figure 22 shows these data as well as the relative intensity curve of the diffuse skylight. Hulburt assumed that this curve is that of the incident radiation outside the atmosphere — in other words, nonselective scattering by the large particles in the clouds.

For his calculations, Hulburt used data obtained in the laboratory on water samples of the spectral absorption and assumed that the spectral scattering was Rayleigh in nature. He also made angular scattering

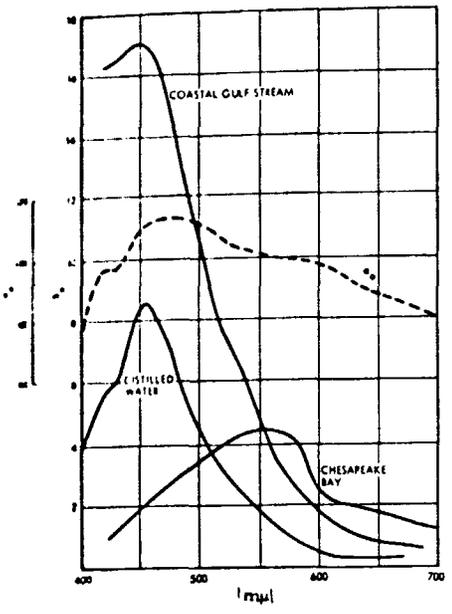

Figure 22. Curves of Hulburt[28] Showing (b_o) Calculated Upward Spectral Intensity of Radiation from Deep Water (Assumed Infinite Depth) for Three Types of Water. a_o is the Spectral Intensity of Diffuse Sunlight.

measurements and determined the quantities η and $(1 - \eta)$ where η is the fraction of the radiation scattered in the forward direction, and of course $(1 - \eta)$ is the backscattered fraction, which is the quantity needed for calculating the upward light from the sea.

He assumed a nonselective, diffuse reflectivity of the ocean surface of $r_d = 0.066$, and calculated a "visible" reflectivity, (R), by integrating over the visible spectrum using the eye response from 0.4μ to 0.7μ. These calculations for a cloudy day are shown in Table VI.

The data of Table VI indicate that about 40 percent of the total upward light from the ocean is due to surface reflection of the diffuse skylight (cloudy day), and 60 percent is the upwelling, or backscattered radiation from beneath the surface. The spectral character of the latter radiation is the "ocean color" of interest to this study.

Table VI. Calculation of Upward Light from Ocean on Cloudy Day, from Hulburt[23]

	No Surface Reflectance	With Surface Reflectance
Distilled Water	0.018	0.036
Gulf Stream	0.047	0.063
Chesapeake Bay	0.035	0.052

Hulburt also gives measured data of the total collimated, "visible" irradiance, i_o for various meteorological conditions as a function of the diffuse irradiance a_o, where $i_o = f\, a_o$. Values of f are given in Table VII.

Using the values for f of Table VII, Hulburt calculated visible reflectance, values (R) of 0.052 for a clear day and obtained values between 0.025 and 0.035 for sunny days with the latter value corresponding to a sun zenith of 90 degrees. His measurements of Chesapeake Bay,

Table VII. Measured Relationship Between Collimated and Diffuse Irradiance Reaching Ocean Surface

Sky	f
All Sun, no sky	infinity
Sunny, clear sky	7
Sunny, hazy sky	3
Sun through thin clouds	1
No Sun, cloudy	0

from 1000-feet altitude showed good agreement with these calculations. Also of note was that the measurements indicated an increase of R of 1 or 2 percent (from 0.05 to 0.06 or 0.07) as the roughness of sea increased. This is in agreement with Powell and Clarke[23].

It is of interest to calculate one effect of wind velocity on the reflected skylight. For an observer looking downward at the ocean from the zenith, the contribution of radiation from the water surface is essentially a specular reflection of the zenith skylight with a calm sea surface. With increasing wind, the sea surface increases in slope (as shown in Figure 15) and the reflected skylight comes from a different portion of the sky. From the data of Figure 15, Figure 23 was constructed. It shows that for wind speeds up to 25 knots, 90 percent of the reflected skylight (to an observer at the zenith) comes from a 15 degree diameter circle around the zenith. Figure 11 shows about a ±10 percent variation in skylight intensity for up to 15 degrees azimuth angles from the zenith.

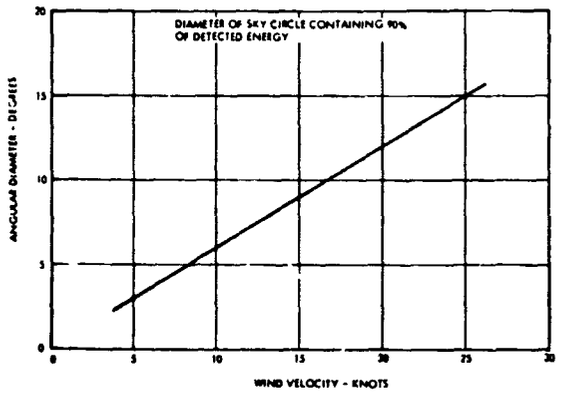

Figure 23. Effect of Surface Roughness on Reflection

4.3 CONCLUSIONS AS TO EFFECT OF WATER SURFACE AND SKY CONDITION ON WATER COLOR

As a result of the various calculations and measurements of the radiation from the sea, what conclusions can be drawn about the effect of the sky conditions, the

water surface conditions, and the water depth on the spectral nature of the sea radiance?

First, outside of the specularly reflected sunlight, the radiance of the sea is composed of two components of approximately equal intensity on days of relatively calm sea surface. These are the diffusely reflected skylight and the so-called backscattered radiation from out of the water. For a rough sea, the reflected skylight component will increase so that it may be up to 50 percent larger than the backscattered component.

The reflected skylight component is selective in spectral character, is primarily a function of the turbidity of the atmosphere, and will affect the spectral nature of the measured sea radiance. Thus any variation in the sky or solar position which might change the intensity or spectral nature of the reflected skylight may be a factor in ocean color measurements.

The total radiation directly upward will vary between about 5 and 10 percent of that received on the surface of the water. This upward radiation is diffuse and not collimated. Again this does not refer to the specular reflection of the collimated sunlight, which for calm seas may be a factor of 500 times the diffuse sea radiance and must not be "seen" by the ocean color spectrometer.

The depth of the water will affect the ocean color as shallow water will show the color of the ocean bottom which will tend to mask the color of the water itself.

Finally, the variation in total irradiance (for small zenith angles) is seven times larger on a clear, sunny day than when completely overcast.

5. THE WATER CHARACTERISTICS

It has been seen that the irradiance obtained by a measuring device pointed at the ocean from a platform above will be composed of the light scattered from the atmospheric molecules, aerosols, and clouds, the light reflection from the ocean surface, and in shallow waters, the ocean floor. This radiation must be considered as background to the signal to be measured (the radiation backscattered from the water itself) and whose spectral nature determines the "color" of the water.

5.1 FACTORS IN WATER WHICH DETERMINE OCEAN COLOR

The clearest waters from either fresh water lakes or the oceans have a deep blue color. This color can be attributed to the selective scattering of light by small particles and water molecules. The blue color gradually changes to a green color as the productivity of the water increases. This change is due to the addition of yellow substances that are directly related to the organic material contained in the water. In addition, some estuarine waters and inland waters are brown and red due to special conditions of the land run-off.

Therefore, the color of ocean water is a measure of the productivity of the water. Information as to water depth may also be obtained from a color measurement.

A detailed discussion of the variables in the water that affect the observed color follows.

5.2 COLOR CATEGORIES OF OCEANS

Ocean waters have been categorized according to the transmission characteristics of visible light. Table VIII lists the wavelength of maximum transmission and the percentage of light of this color transmitted in five different types of ocean, as taken from Jerlov.[29]

Roughly speaking, sea water is translucent for visible radiation only, and most penetrable for just the wavelengths that are useful to plants. In general, the less clear the water, the more the shifting of "surviving" wavelengths toward the longer waves, the green and yellow.

Table VIII. Wavelength of Maximum Transmission and the Percentage of Light of This Color Transmitted In Five Different Types of Ocean (From Jerlov[29])

Types of Ocean Water	Wavelength of Maximum Transmission	Percent Transmission Per Meter
Clearest oceans	470	98.1
Average oceans	475	89.0
Clearest coastal	500	88.6
Average coastal	550	72.4
Average inshore	600	60.8

The familiar blue color of the sea is due to scattering among water molecules and small particles. The less other material there is in the water the bluer it appears. Hence, blueness in the ocean is indicative of poverty. The green color of great coastal waters of the sea has been attributed to the presence of "yellow substances". Figure 24 taken from Kalle[30] shows in a qualitative fashion a relationship between the "visible depth" of ocean water and the causes of the color of the ocean. On the right hand side is the maximum wavelength of the color and the Forell Scale number associated with the "visible depth".

5.2.1 Blue Color of Clear Waters

Referring to Figure 24 the blueness of the clearest ocean and lake waters (visible depth to 60 meters) is attributed wholly to the selective scattering of light by small particles, (according to Kalle[30] and Jerlov[29]); however, the properties of clear water are such that this conclusion is not obvious.

The transmission of filtered ocean water, double distilled water, (from Clark and James[31]), and the clearest natural water (from Crater Lake as measured by Smith and Tyler[32]), is shown in Figure 25. The curves are nearly identical indicating that the dissolved salts in the

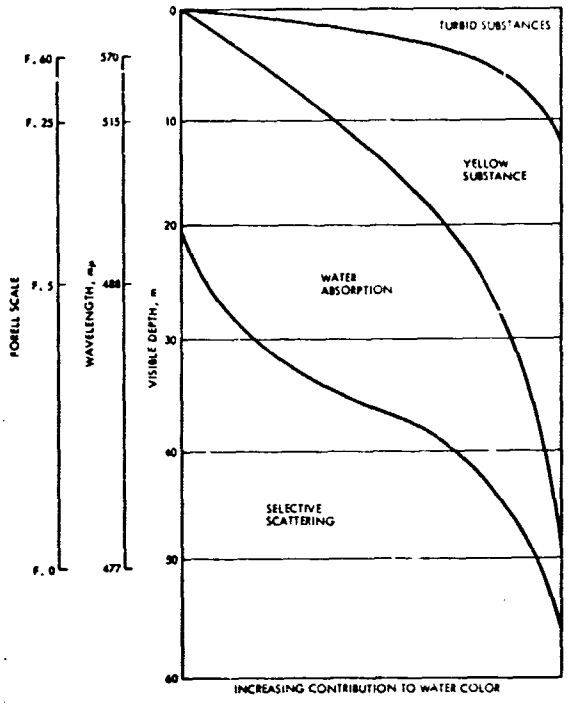

Figure 24. Relationship Between "Visible Depth" and Source of Color of Sea Water, Kalle[30]

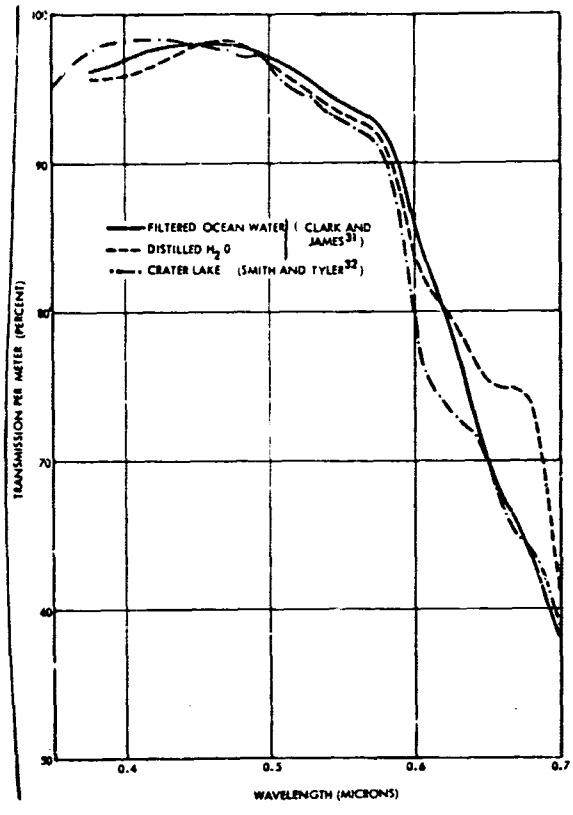

Figure 25. Percent Transmission of Clear Waters

clearest ocean waters have little effect on its transmission of visible light. The peak of the transmission curve for clear water is at about 475 mμ, a blue-green color.

The important feature of Figure 25 is the strong absorption band of water starting at 585 mμ and continuing strongly into the red portion of the spectrum. The attenuation of light by sea water is, however, a combination of absorption and scattering. Duntley[26] states that the scattering of light in the sea, due to biological organisms and large particles, is predominately Mie scattering, and is nonselective with wavelength. In addition, he states that the spectral variation in attenuation of light by water, such as that of Figure 25, is due almost wholly to selective absorption.

Jerlov[29] indicates a solution to the apparent contradiction by showing that the backscattered light, which determines the color of the sea, is selectively scattered, although the predominant scattering is nonselective.

It is because particles, either molecules or various solutes, are present, and although the total small particle scattering is much less than the large particle scattering, the Rayleigh backscatter predominates because the Mie backscatter is predominantly in the forward direction.

Figure 26 (Dawson and Hulburt[33]) and Figure 27 (Jerlov[34]) show the volume scattering function due to ocean water of green and blue light respectively.

The curves show a pronounced forward scattering, which indicates that the particles are fairly large. An application of the Mie theory suggests a size on the order of 10μ (Jerlov[34]). Thus, the particle scattering is not very selective to wavelength as a comparison of the two figures shown. The lower curves in Figures 26 and 27 are the theoretical scattering of pure water computed from the Rayleigh formulae.

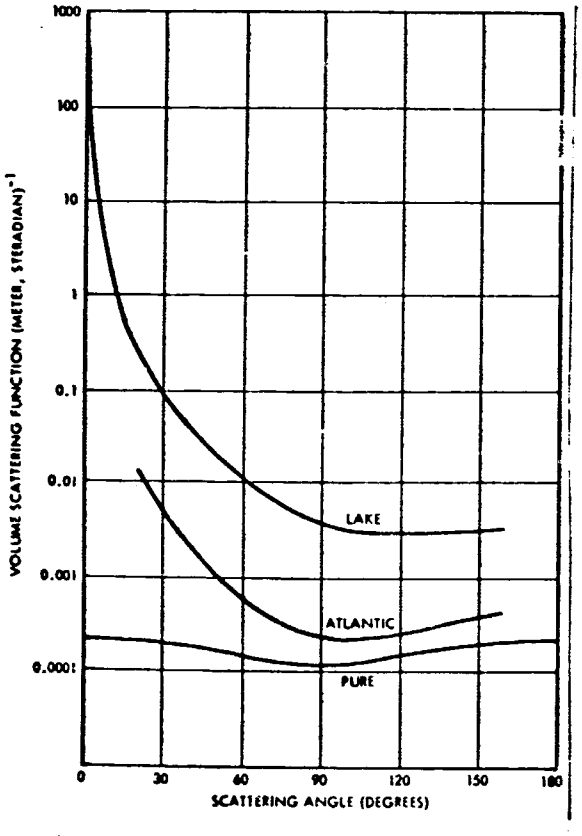

Figure 26. Volume Scattering Function of Green Light by Pure, Atlantic, and Lake Waters, Dawson and Hulburt[33]

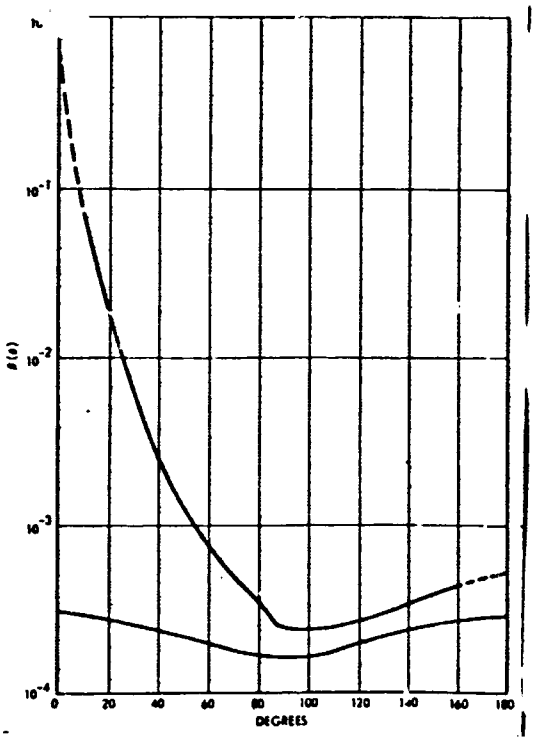

Figure 27. Volume Scattering Function for Ocean Water (Upper Curve) and Pure Water (Lower Curve) for Blue Light (465 mμ) Jerlov[29]

The scattering of distilled water resembles that of ocean water rather than pure water as shown by Figures 28 and 29 from (Duntley[26] and Hulburt[28]), respectively. Hulburt noted that there is no compelling reason why the scattering of water should conform with a simple theory.

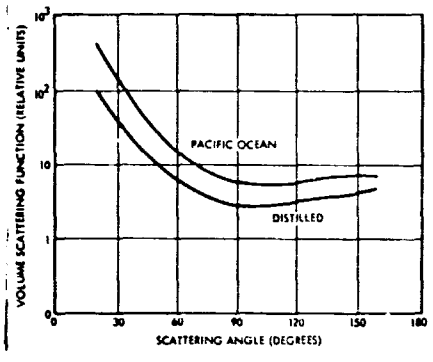

Figure 28. Volume Scattering Function of Pacific Ocean and Distilled Water, Duntley[26]

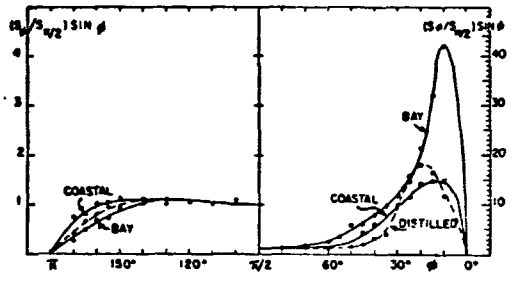

Figure 29. Volume Scattering Function of Coastal, Bay, and Distilled Water, Hulburt[28]

The spectrum of the scattered light of distilled water is shown in Figure 30 (Hulburt[28]). The fact that there is little selective scattering coincides with the previous scattering angle observations. Even though the selective scattering is small, it is effected without losses and thus predominates. The nonselective scattering is mostly forward scattering and gives little contribution to the upwardly traveling light. The predominance of selective scattering in the upward component of daylight is well developed in the extremely clear water of the Sargasso Sea and the East Mediterranean. But in ocean water of normal transparency where big particles are more abundant, the multiple selective scattering is extinguished by absorption, and the brilliant blue color is lost.

5.2.2 Green Color of Fertile Waters

The change of the color of ocean water from blue to green has been attributed to the addition of a yellow substance (first referred to by Kalle[30]) which selectively absorbs the red and blue portions of the spectrum. The nature of the yellow substance is not precisely understood. Accompanying the yellow substance is observed a fluorescence which, however, seems to have a minor influence on the optical properties of ocean water. The absorption curve necessary to produce the green color is shown in Figure 31, from Jerlov[34].

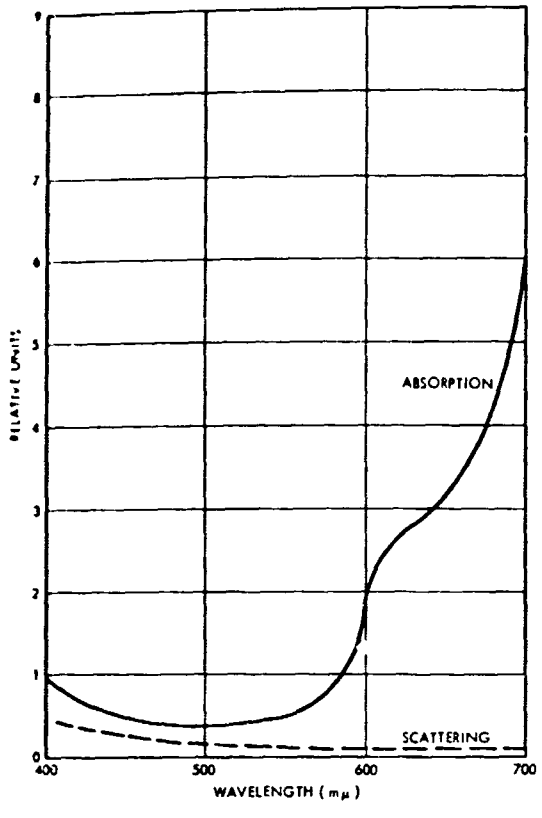

Figure 30. Absorption and Scattering of Distilled Water, Hulburt[21]

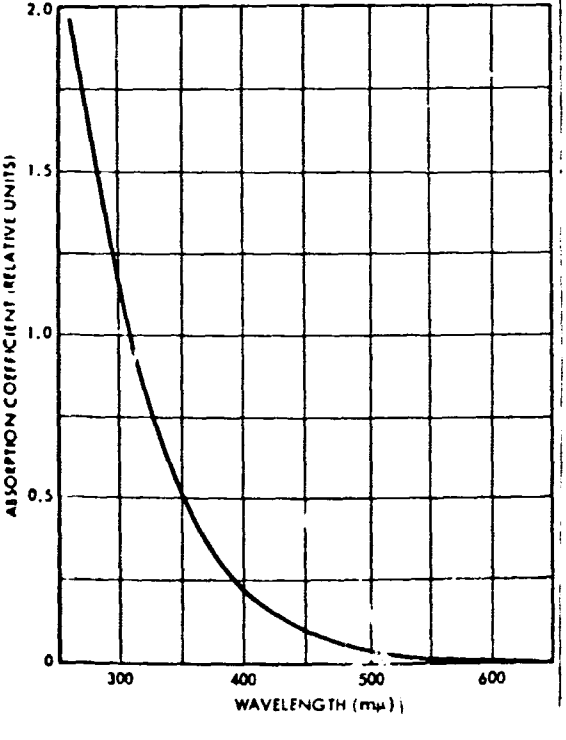

Figure 31. Absorption Curve of Yellow Substance, Jerlov[29]

Kalle[30] and Jerlov[34] conclude that the yellow substance is dissolved and formed from free carbohydrates and free amino acids, i.e., where organic matter is disintegrating. The end product is composed of carbohydrate-humic acids of melanoidines which are yellow and fairly stable in sea water. Figure 32 is a plot of fluorescence, ϕ, against the 90 degree scattering function β, for stations in the Mediterrane. at various depths, as taken from Ivanoff[35]. The crosses are for data taken at depths less than or equal to 75 meters. The circles are for data taken at depths greater than 75 meters. Above 75 meters there is a correlation coefficient of 0.81, but below 75 meters there is no correlation. A possible explanation is that the fluorescence is due to the decomposition products of suspended matter, and consequently fluorescence increases with the amount of suspended matter for those depths where decomposition takes place. At greater depths fluorescence remains constant.

Table IX is a list of values of fluorescence and scattering for one particular station in the Mediterranean, also from Ivanoff[35]. He suggests that since the fluorescence measurements were more stable

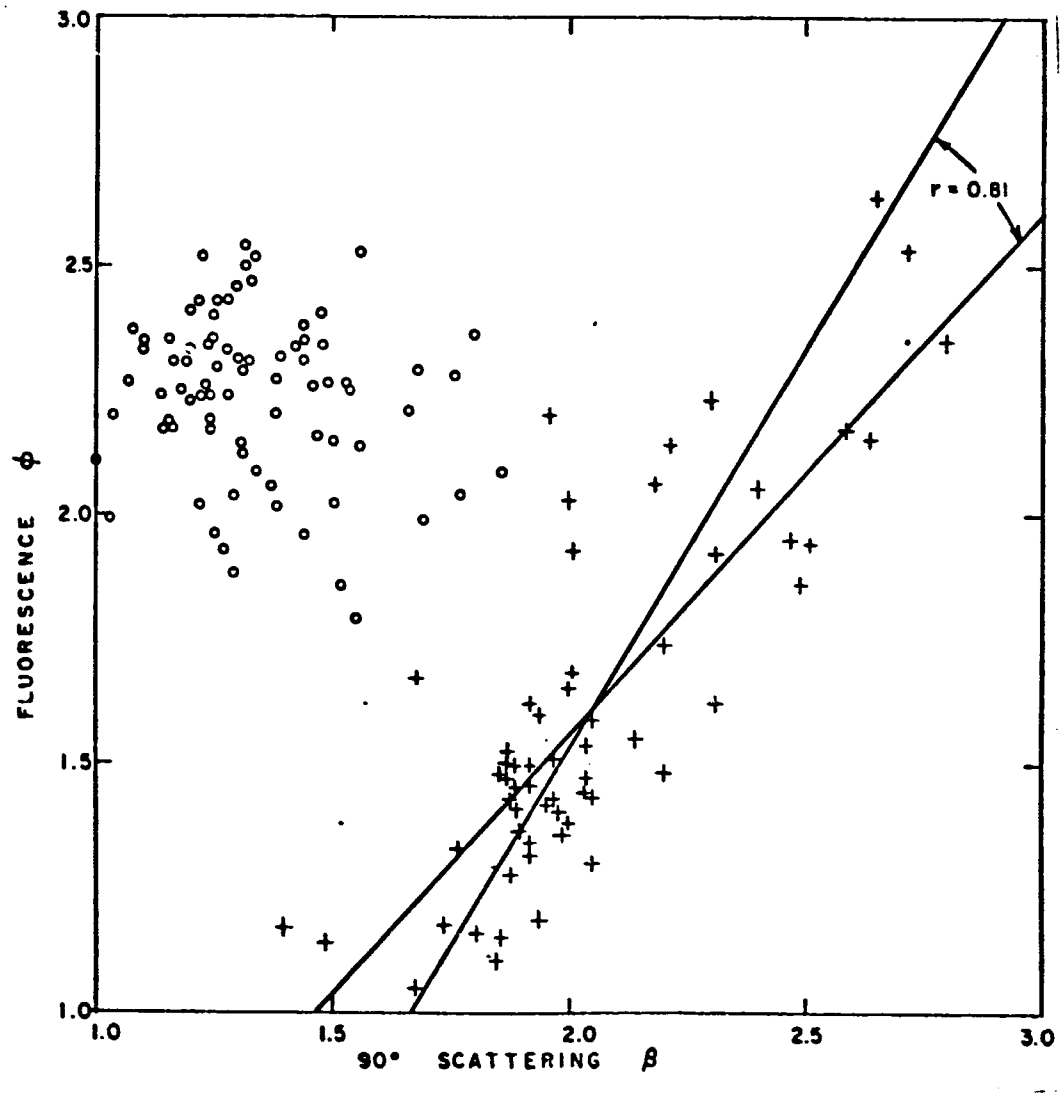

Figure 32. Fluorescence ϕ Plotted Against Scattering β for Measurements of Many Depths, Ivanoff[35]

than the scattering measurements the fluorescence is due to dissolved substances rather than suspended matter.

Recently Yentsch[36] suggested that the yellow substance is not dissolved in the water, but rather the photosynthetic pigments of phytoplankton. Figure 33 (taken from Yentsch[36]) shows the absorption spectrums of various living phytoplankton. They all exhibit an absorption minimum in the green, strong combined cholorophyll and carotenoid absorption in the blue, and the red absorption by chlorophyll a.

Table IX. Values of Scattering and Fluorescence At Various Depths, From Ivanoff[35]

Depth, meters	Scattering β	Fluorescence Φ
1	1.96	$0.141 < \Phi < 0.147$
5	1.98	
10	2.04	
25	1.88	
50	2.51	0.195
75	1.60	0.205
100	1.47	0.215
125	1.67	———
150	1.48	0.240

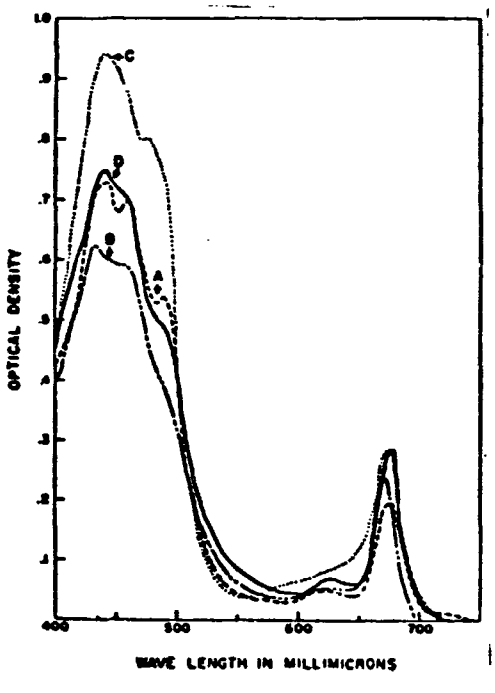

Figure 33. Pigment Spectra of Living Phytoplankton, a) Diatom Cyclotella sp., b) Dinoflagellate, Amphidium sp., c) green Flagellate Chlamydomonas, d) Natural population Sampled from Woods Hole Waters, Yentsch[36]

The absorption curves of various concentrations of plant pigments in pure water shown in Figure 34, also from Yentsch[36], shows the shift to the green of increasing concentrations. He filtered ocean water with successively smaller filters and examined the filtrate at each step.

Figure 35 (Yentsch[37]) shows the relative attenuance of particulate matter of various sizes. This indicates that a large fraction of the

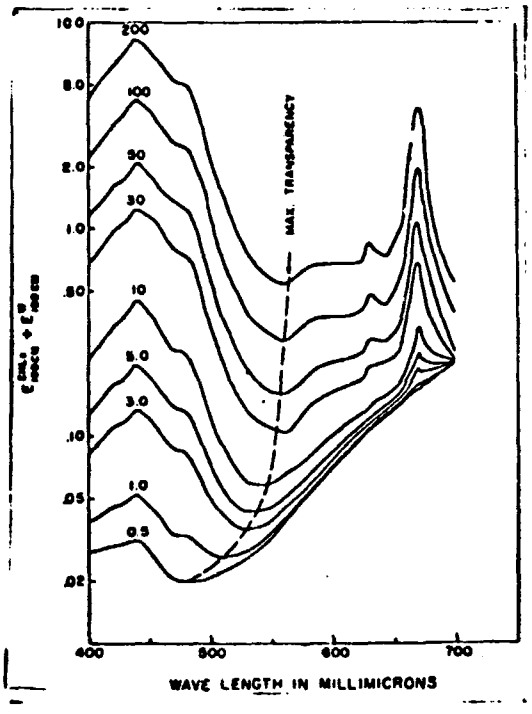

Figure 34. Combined Absorption Coefficients for Pure Water and Plant Pigments. Numbers Adjacent the Curves Indicate the Chlorophyll Concentration in mg/m^3, Yentsch[36]

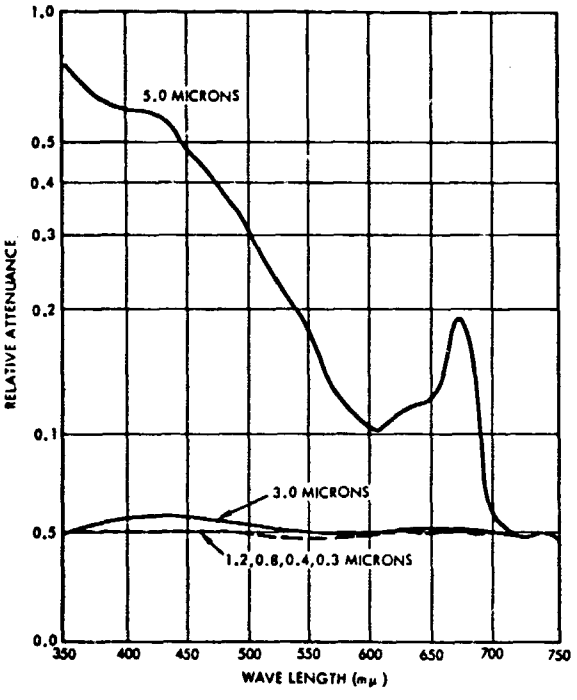

Figure 35. Relative Attenuance of Particulate Matter of Various Sizes in Woods Hole Waters, Yentsch[37]

yellow substance is either particulate or is absorbed by particles. The absorption curve is similar in shape to the necessary curve required to produce the green color. An inverse relationship has been noted between the disappearance of chloroplastic pigments and the production of the ultraviolet yellow absorbing substances. It suggests that the yellow compounds are derived from the protein carrier originally coupled to the chlorophyll chromophore.

5.2.3 Colors of Turbid Waters

The color of turbid waters has been described variously as red, brown, and white. The color of these waters is principally due to land run-off and live or decayed organisms in the water.

The "red seas" which appear to be a sea of blood have a high concentration of red shrimp. Diatoms in enormous numbers give a yellowish color to the water. Orange casts to water have been attributed to a one-celled plant-like organism, Gymnodinium flavium. River and lake waters sometimes exhibit a yellow or brown color. The exact source of this color is not known but they have been referred to in general terms as tannins, lignins, and humus.

6. CHLOROPHYLL A AS AN INDEX OF OCEAN PRODUCTIVITY

Tyler[38] has reported measurements in ocean waters of the chlorophyll content with the purpose of providing a capability of following changes in phytoplankton populations. Nutrients were added to a pond of water which was then seeded with a mixed population of phytoplankton. Figure 36 shows the concentration of chlorophyll a as a function of time. Figure 37 shows some of his spectroradiometric curves taken during this time. The strength of the absorption band at 680 mμ indicates the increases and decreases in the chlorophyll. Tyler[38] also measured absorption bands in ocean water at 410 and 515 mμ, although the band at 680 mμ is by far the strongest.

Holmes[39] measured chlorophyll a in the Pacific and found values ranging from 10.2 to 0.72 mg/m^3 in rich areas with lower values down to 0.037 mg/m^3 in poor areas. Recently, Blackburn[40] measured amounts of chlorophyll a, zooplankton, and copepods at 36 station-pairs

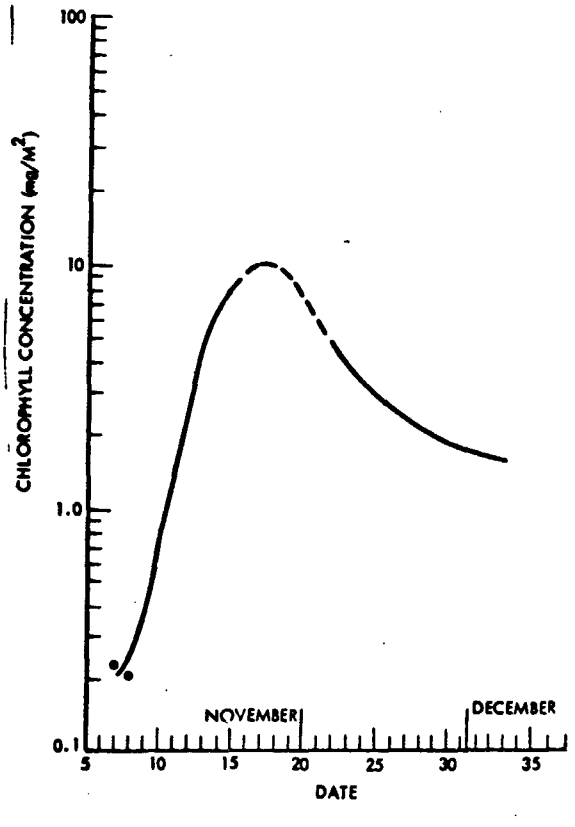

Figure 36. Concentration of Chlorophyll-a as a Function of Time, Tyler[38]

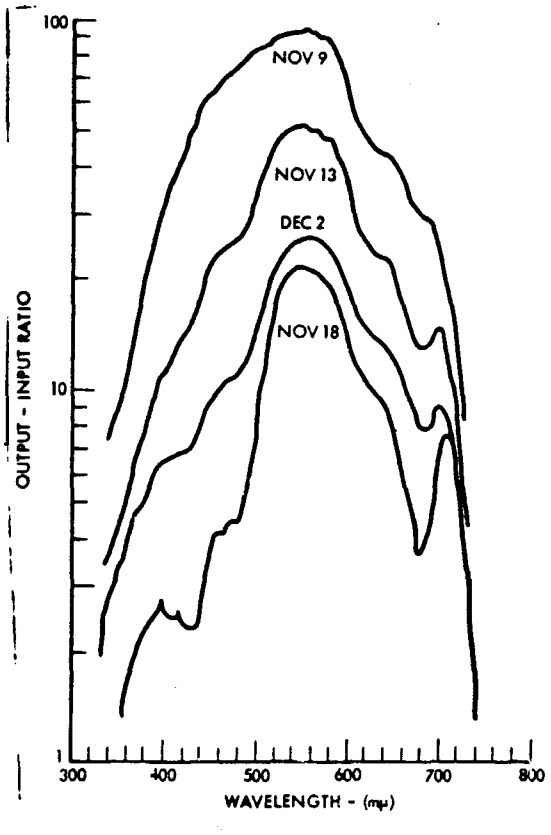

Figure 37. Selected Output/Input Curves Arranged for Comparison. Because Data Were Obtained Under Varied Lighting Conditions, These Curves are not Plotted in Correct Ordinate Relationship to One Another. Tyler[38]

in the eastern tropical Pacific. A positive correlation was found between the chlorophyll content and these ocean "crops."

Yentsch[36] suggests that the quantity of chlorophyll can be used as an index of the total phytoplankton pigment in the oceans. Therefore, the relationship between chlorophyll content and "color" of the oceans was investigated by making calculations of the spectral nature of the upward flux from waters.

6.1 CALCULATIONS OF WATER REFLECTANCE

The spectral nature of the backscattered radiation from the sea is a function of four things, i.e., 1) the spectral absorption of the water and its constituents; 2) the spectral scattering due to both the water molecules and the particles in the water; 3) the directional nature of this scattering; and the nature of the incident solar energy, which is both direct and diffuse. The total upward flux from the water also contains that radiation reflected from the surface.

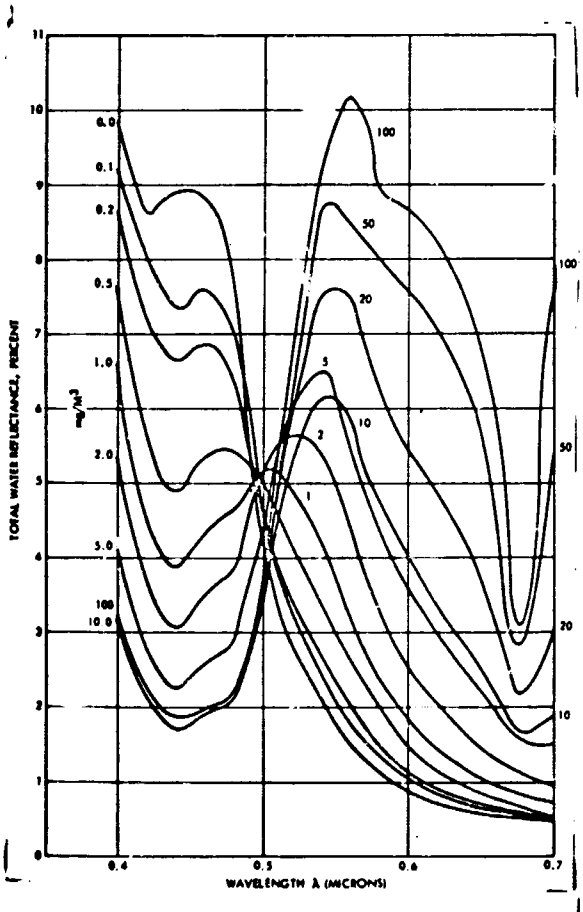

Figure 38. Calculated Spectral Reflectance of Deep Ocean with Varying Amounts of Chlorophyll, Clear Sunny Day – 45° Solar Zenith Includes Surface Reflection from Smooth Ocean with Turbid Atmosphere Above

Appendix A gives the equations used in the calculations of upward flux, a definition of the various parameters and their assumed values used in the calculations.

Figure 38 shows the spectral reflectance, R, of the deep ocean for a sunny day with the sun at a 45 degree zenith angle. Each curve represents a different chlorophyll concentration, varying from zero to 100 mg/m^3. These reflectance data are composed of both backscattered light and that diffuse radiation reflected from a smooth ocean surface. The atmosphere above is assumed to be turbid (T = 4.5), which affects the spectral nature of both the downward and upward radiation at the surface.

The curves of Figure 38 show the change from the blue color, expected for clear water with little or no chlorophyll, to the predominant green or yellow colors, for the heavy concentration.

Because of the many assumptions made in the calculations, it is not expected that a measurement of chlorophyll concentration and upward flux in a particular part of the ocean should correlate exactly with the data of Figure 38. These curves should prove of use as a model, however, from which various conclusions may be drawn, particularly in the design of an ocean color measuring system. It is of interest to compare these calculations with some measured data.

Figure 39 shows a comparison of three of these curves of Figure 38 with measurement data. Curve 1, of Figure 39, is calculated for distilled water. It is compared with two curves measured by Jerlov[29] for two sun angles in clear Indian Ocean water, which should correspond closely to distilled water. Tyler and Smith[41] measured the upward flux from water at various depths. Values at 4 and 8 meters from water with a surface concentration of chlorophyll a of 2.6 mg/m^3 are shown and compared with calculated curves for both the 2.0 and 5.0 mg/m^3 concentrations.

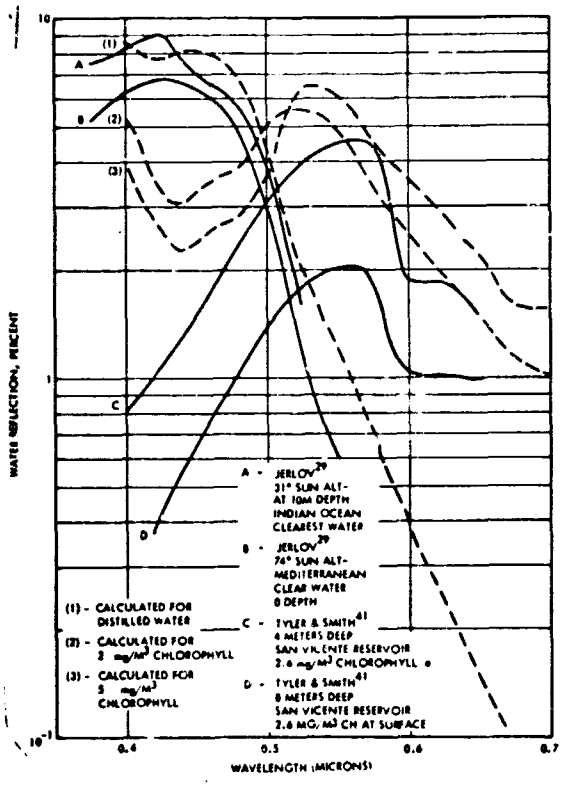

Figure 39. Comparison Between Measured and Calculated Water Reflectance

6.2 CALCULATION OF ATMOSPHERIC CONTRIBUTION TO MEASURED RADIATION FROM OCEAN

In order to calculate the expected total upcoming radiation measured by a spectrometer in an aircraft or spacecraft, the contribution from the atmosphere must be considered.

Fraser[42, 43] has calculated the total intensity of scattered radiation outward from the earth and atmosphere for various model atmospheres. Figure 40 shows his data as calculated for a Rayleigh Atmosphere,

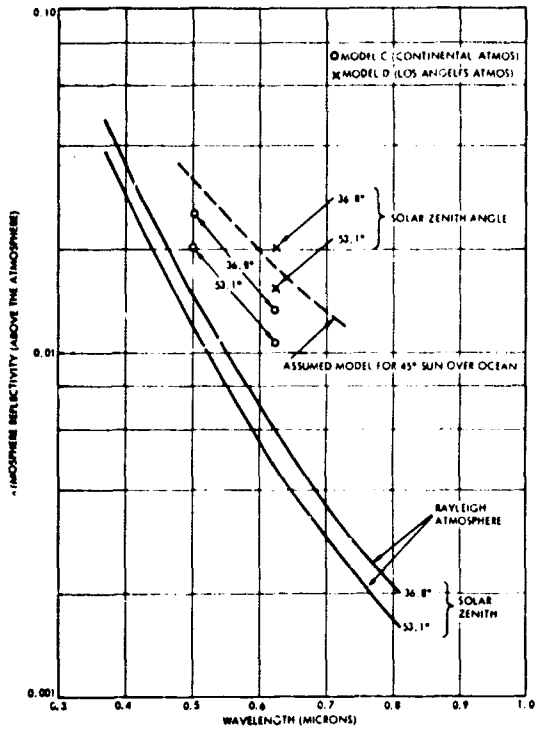

Figure 40. Calculated Spectral Reflectivity of Total Atmospheric (Earth Albedo = 0) for Various Model Atmospheres for Viewing the Nadir, Fraser[42,43]

a continental atmosphere (Model C) and for (Model D), designated a Los Angeles atmosphere, which contains more large particles than the continental and should best simulate the ocean conditions. The spectral nature of the atmospheric reflectivity, for the nadir direction, with a 45 degree sun, is obtained by extrapolating as shown in Figure 40.

The upward flux is determined by multiplying this shown curve by the absolute spectral irradiance above the atmosphere (m = 0, from Figure 1).

It is of interest to know the contribution from each layer of the atmosphere to this total upward flux, so that a distinction can be made between what would be measured from an aircraft, at various altitudes, and from a spacecraft. This was calculated by the following method.

The amount of solar radiation scattered upward by a layer, 1, of the atmosphere is assumed proportional to $(1 - e^{-\tau_1 \sec\theta})$, where τ_1 is the optical thickness of the layer and θ the solar zenith angle. Thus the percentage of the total skylight at the nadir for any altitude, H, is

$$100 \sum_{o}^{H} \left(1 - e^{-\tau_1 \sec\theta}\right) / \sum_{o}^{\infty} \left(1 - e^{-\tau_1 \sec\theta}\right)$$

Figure 41 is a plot of this percentage for the Rayleigh atmosphere and the Elterman[44] standard atmosphere for various wavelengths. The Los Angeles atmosphere, used by Fraser[43] is shown plotted for 0.625μ. Figure 42 shows these data plotted for altitudes of 1, 3, 10, and 30 km. The Los Angeles type atmosphere is extrapolated to follow the data of Elterman[44]. The curves of Figure 41 and 42, therefore, when used

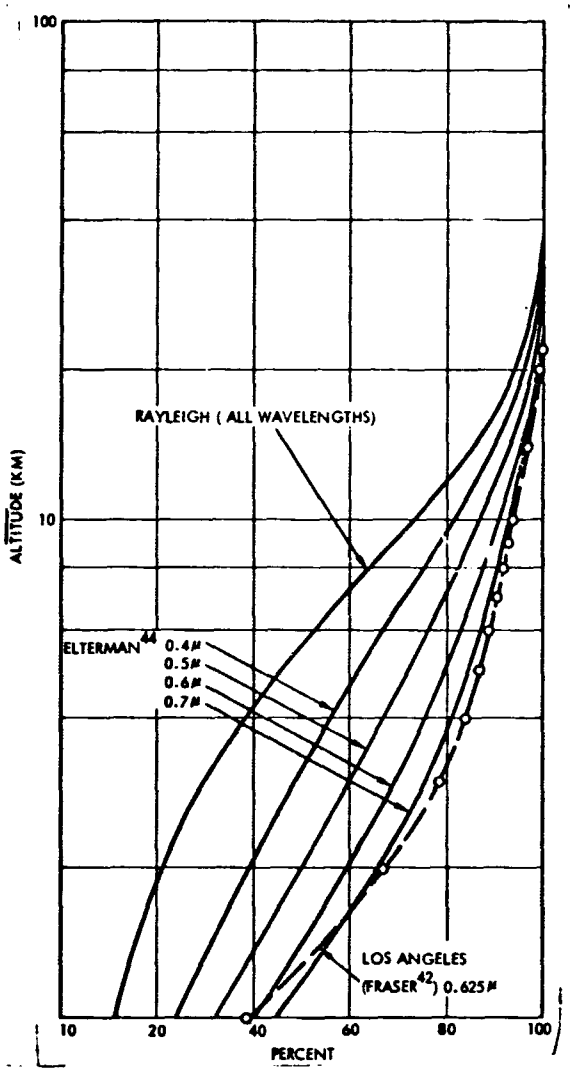

Figure 41. Percentage of Total Earth Airlight Toward Nadir for Various Model Atmospheres and Wavelengths (45° Sun)

to modify the data in Figure 40 will yield a spectral atmospheric reflectance at the nadir for a turbid atmosphere (Los Angeles), and a Rayleigh atmosphere, respectively.

6.3 TOTAL UPWARD FLUX FROM OCEAN AND ATMOSPHERE

Using the data of Elterman[44], the spectral transmissivity for a turbid atmosphere in the zenith direction was determined. It is shown in Figure 43a for the altitudes of interest above, and Figure 43b gives the spectral transmissivity for a Rayleigh atmosphere.

Figures 44 and 45 show the upward flux in π steradians (radiance) at various altitudes, with the separate contribution from water (clear — no chlorophyll) and atmosphere exhibited for a turbid (Model D), and a Rayleigh atmosphere, respectively.

Figure 46 gives the total spectral radiance of the nadir at various altitudes and shows the difference between the radiance for clear water with no chlorophyll, and that obtained with 0.2 mg/m^3 content of chlorophyll.

Figure 47 shows the expected difference in radiance between the two extreme atmospheric conditions of a Rayleigh and a turbid (T = 4.5) condition. Although the magnitudes are different (approximately 40 percent higher for the turbid atmosphere) the relative difference between the clear and 0.2 mg/m^3 chlorophyll cases is not significant. For example, at 0.46μ, the difference in radiance for the Rayleigh atmosphere is about

20 $w/m^2/\mu/\pi$ ster versus a value of 17 for the turbid atmosphere. This suggests, if it is assumed that a difference of 0. 2 mg/m^3 of chlorophyll is the required sensitivity of the measuring instrument, that corrections for the type of atmosphere may not be of prime importance in the measurement of ocean color from a satellite.

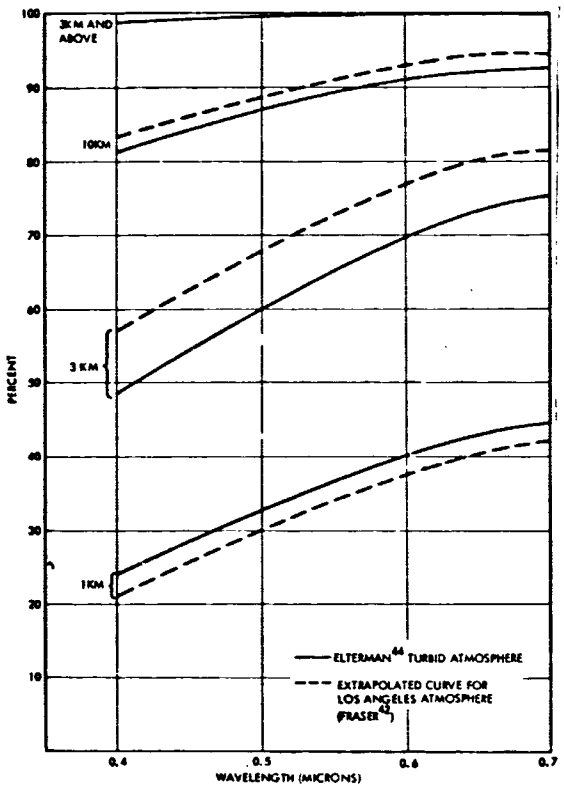

Figure 42. Spectral Percentage of Total Upward Airlight from Atmosphere Reaching Particular Attitude

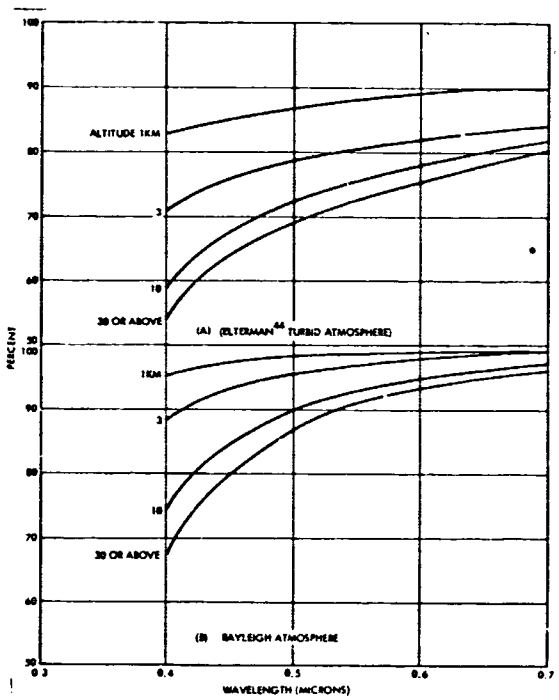

Figure 43. Percentage Transmissivity in Zenith Direction for Two Model Atmospheres

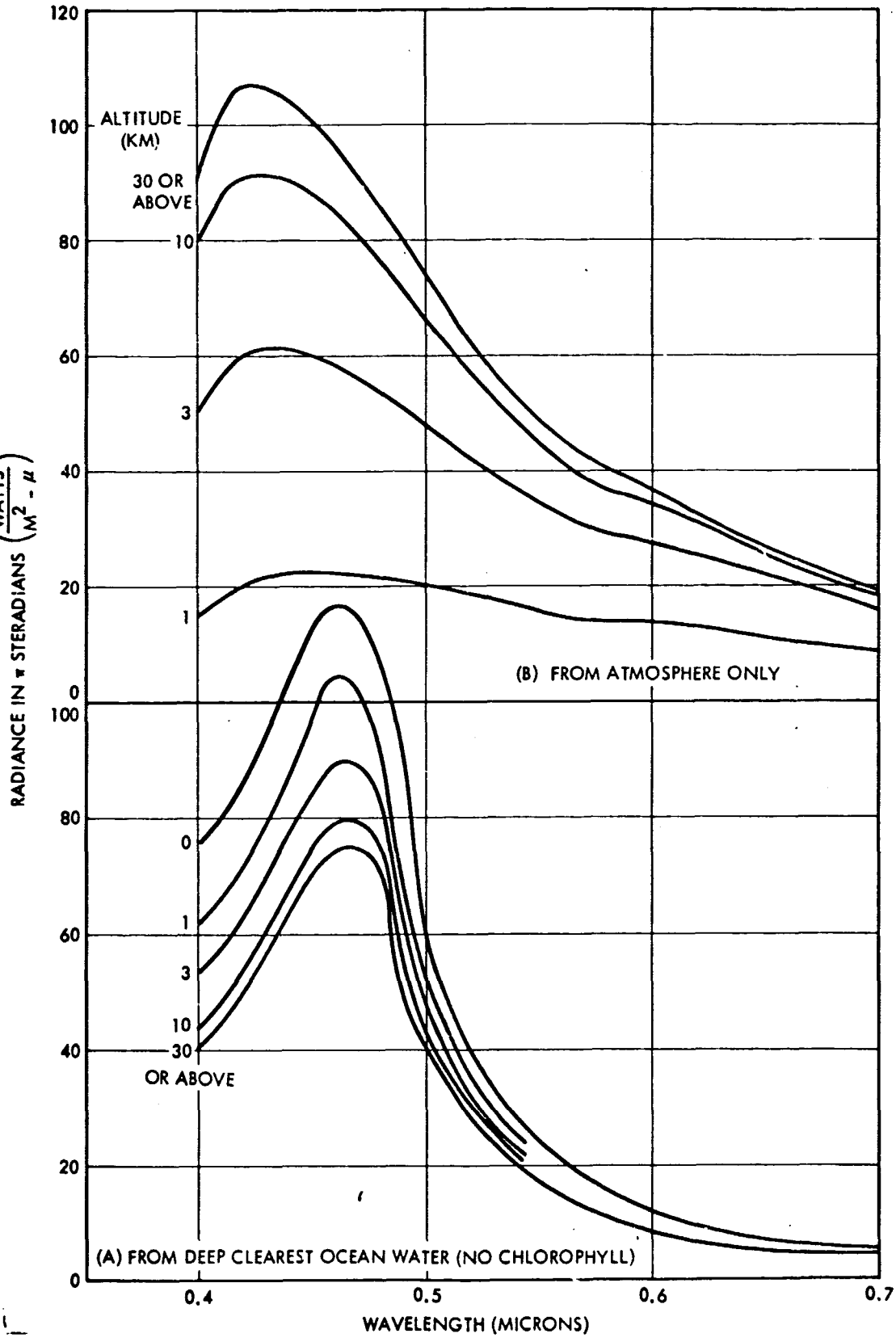

Figure 44. Spectral Upward Flux from Water and Atmosphere at Various Altitudes, Model D (Fraser[42]), Turbid Atmosphere (45° Sun) – Smooth Ocean

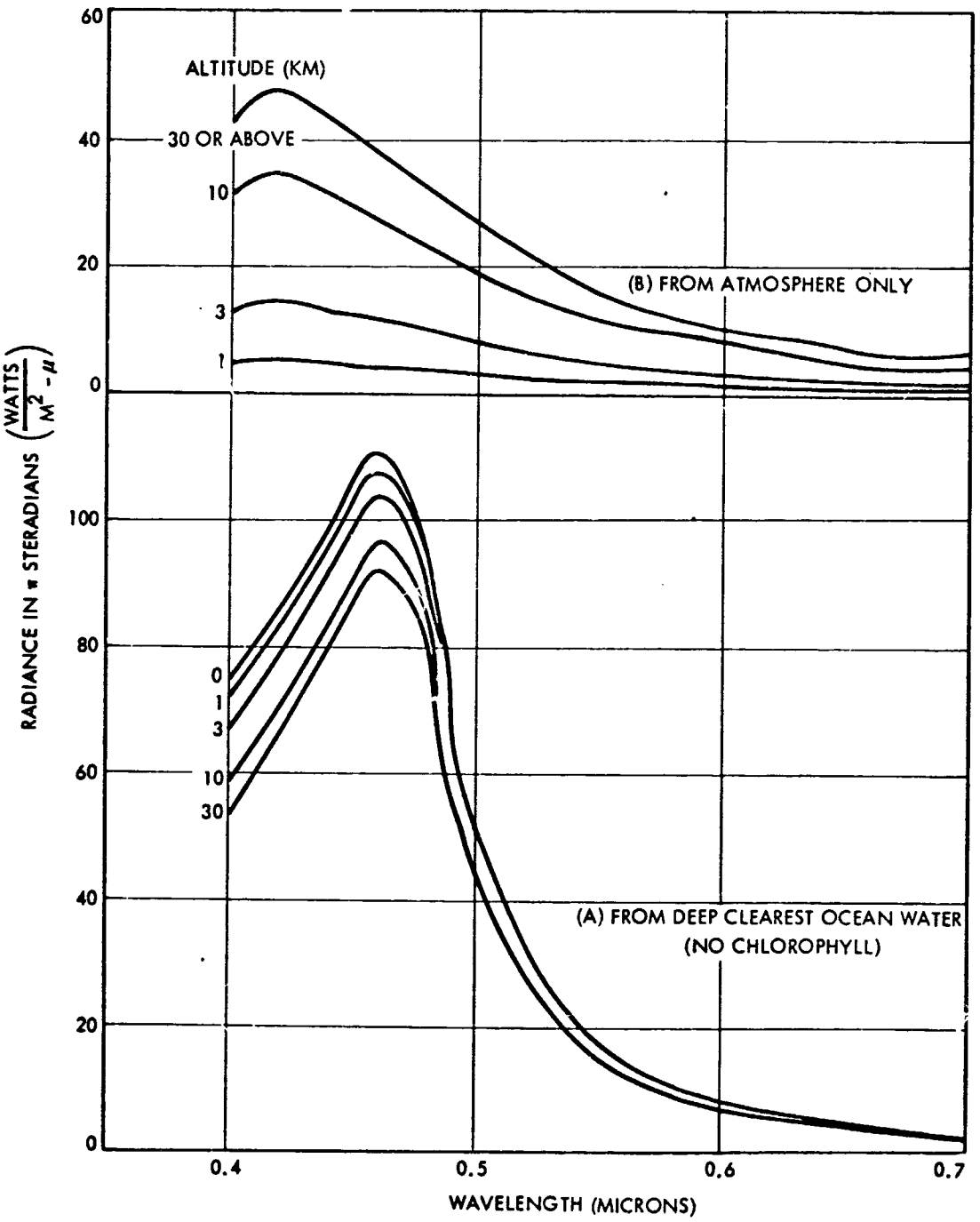

Figure 45. Radiance Contribution from Water and Atmosphere at Various Altitudes – Rayleigh Atmosphere (45° Sun) – Smooth Ocean

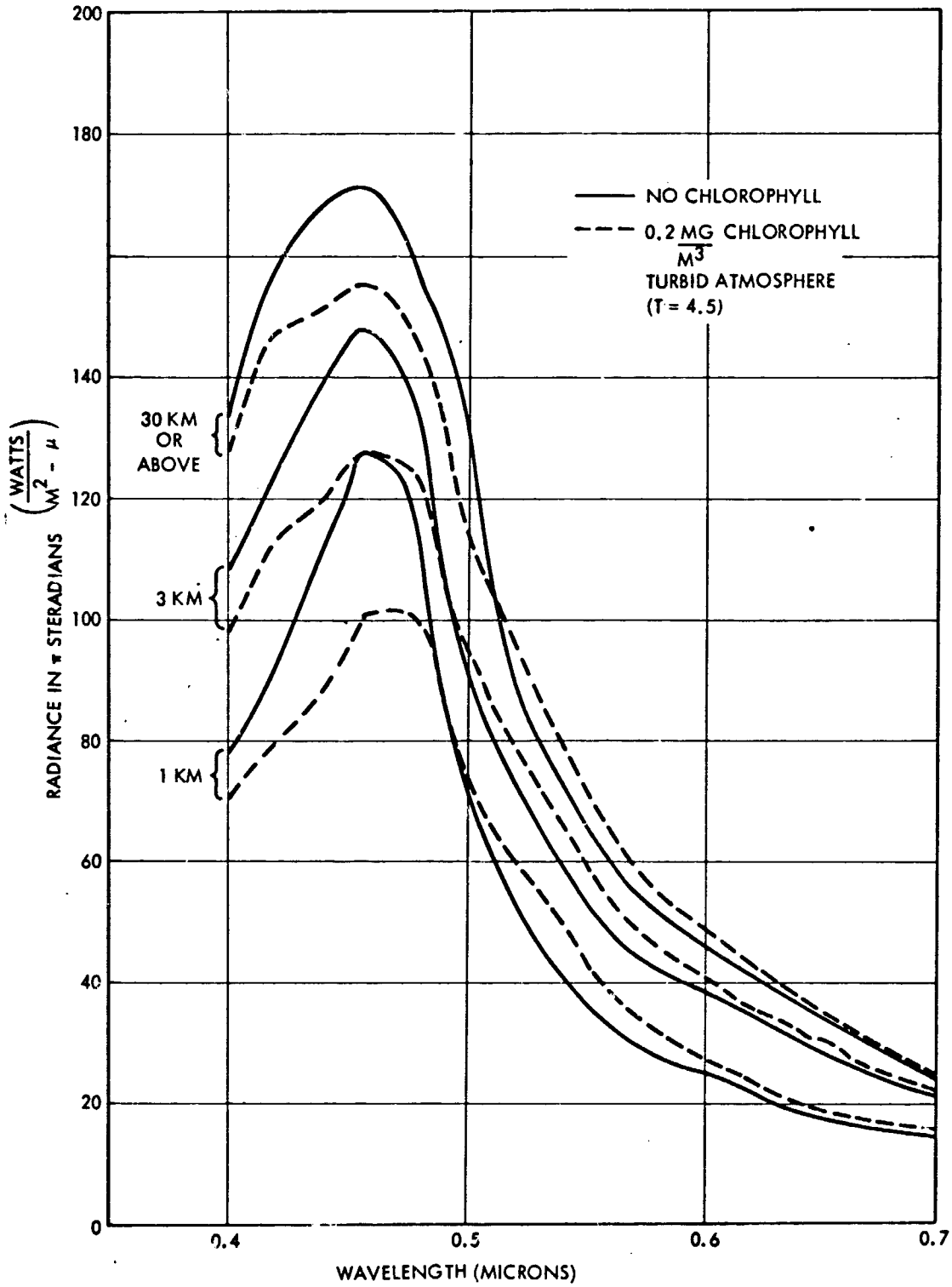

Figure 46. Total Spectral Radiance at Nadir from Various Altitudes Above Deep Ocean

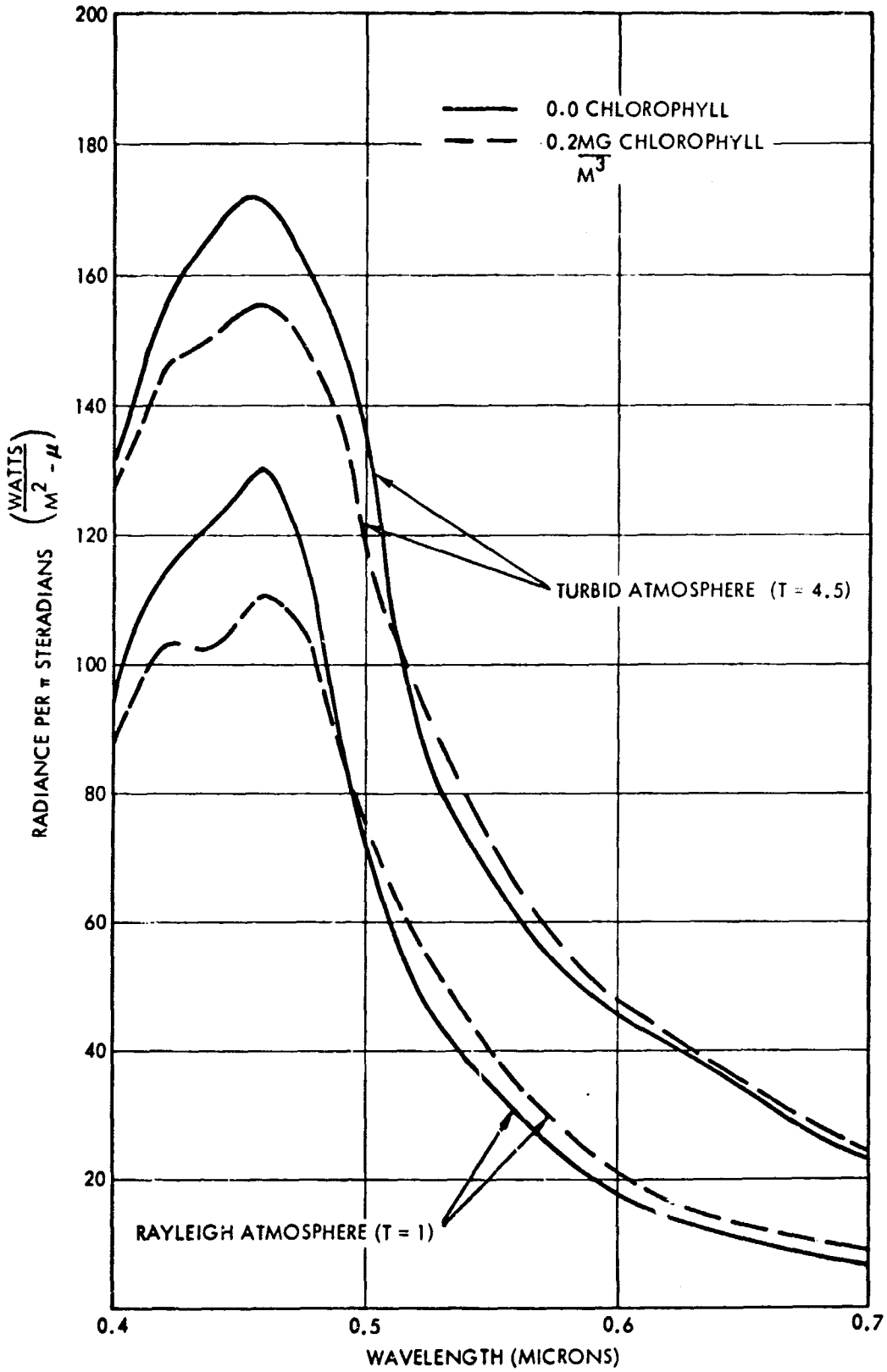

Figure 47. Spectral Radiance Above the Atmosphere at the Nadir for the Extremes in Atmosphere

7. SENSOR SPECIFICATIONS FOR MEASURING OCEAN COLOR

On the basis of the data presented in Figure 47, the following specifications for a WISP (Wide-range Image Spectrophotometer) to measure ocean color are given.

7.1 SPECTRAL REGION OF INTEREST – 0.40 to 0.70 micron

In this region (see Figure 47,) the difference in chlorophyll concentration is most clearly demonstrated, particularly between 0.4 and 0.5μ. This is due to the strong absorption centered at 0.44μ (see Figure A-1). The relatively stronger band at 0.67μ is not as effective because the water itself is more highly absorbent here. However, for high concentrations of chlorophyll, as between 10 and 100 mg/m^3, the differences may be apparent (see Figure 38). Also, the peak of the curves occur beyond 0.5μ for the chlorophyll concentrations above 1 mg/m^3 and it is of importance to measure the position of the peak.

7.2 NOMINAL SPECTRAL RADIANCE – 50 w/m^2/μ/ster

The peak of the curves of Figure 47 give this value for the expected upward radiance for the nadir above the atmosphere. Although not specifically calculated here, the water reflectance data of Figure 38 indicate equivalent values for the peaks obtained beyond 0.5μ for water with high chlorophyll concentrations.

7.3 MAXIMUM SPECTRAL RADIANCE – 300 w/m^2/μ/ster

The data plotted in Figure 47 were calculated for a clear sky and correspond to approximately a 10 percent reflectance. Assume, because of clouds, that the earth has an overall reflectance (albedo) of 0.60. Thus, modifying the data of Figure 2, (m = 0), by this factor yields a maximum spectral radiance of 300 watt/meter^2/ster/μ.

7.4 MEASUREMENT ACCURACY – 3.0 w/m^2/ster/μ (0.4 to 0.5μ)
1.5 w/m^2/ster/μ (0.5 to 0.6μ)

The required measurable variation for the spectral region between 0.4 and 0.5μ for the 0.0 and 0.2 mg/m^3 curves of Figure 47 is about 10 watt/m^2/π ster/μ or 3.0 w/m^2/ster/μ. Beyond 0.5μ the differences

become smaller as the wavelength increases, so that an accuracy in this part of the spectrum is increased by a factor of two. Between 0.6 and 0.7μ, the measurement accuracy achieved will be greater than the values quoted above because of decreasing quantum efficiency of the tube and decreasing solar energy.

7.5 PRECISION (REPEATIBILITY) – $\begin{matrix} 1.5\ w/m^2/ster/\mu\ (0.4\ to\ 0.5\mu) \\ 0.75\ w/m^2/ster/\mu\ (0.5\ to\ 0.7\mu) \end{matrix}$

A precision of one-half the measurement accuracy corresponds to a value of 0.1 mg/m^3 in the amount of chlorophyll concentration at a concentration of 0.2 mg/m^3.

7.6 SPECTRAL BANDPASS ($\Delta\lambda$) – 0.02 micron (200 Å)

The majority of the calculations which resulted in the curves of Figures 44, 45, 46, 47, for example, were made with values at intervals of 0.2μ. Therefore, it is expected that variations in these curves over wavelength intervals of less than 0.02μ should be smoothed out.

The basic data on which these calculations were made are the absorption curves of Figure A-1 and the scattering data of Figure A-2. The absorption coefficient data could be reproduced to a sufficient accuracy by using data obtained every 0.02μ. The scattering curves, although highly idealized for these calculations, should by their nature (the scattering is performed by many particles, ranging from molecular size to those of diameters somewhat larger than the wavelength of interest) yield smooth curves over the spectral intervals of interest. Data of Tyler and Smith[41], taken every 0.1μ for the upwelling and downwelling of radiation in water, do not indicate any need for a spectral bandpass of less than 0.2μ in water color measurements.

7.7 NUMBER OF SPECTRAL BANDS (N_s) – 15

A spectral resolution of 0.02μ over the region of 0.4 and 0.7μ results in 15 adjacent spectral bands.

The necessary additional parameters required to define a system are the ground resolution (Δl) satellite altitude (H), angular field of view (θ) and the period (time) to cover the earth (P). Values of H below 250 nautical miles are not of significance because of rapidly decreasing

satellite lifetimes. The following subsection outlines and discusses the tradeoff performed to arrive at design values of the parameters.

7.8 PARAMETER TRADEOFF STUDY

On the basis of simplicity in circuitry and ease of calibration, an image dissector tube (IDT) is considered as the first choice for an image tube. If the calculations indicate that enough sensitivity is maintained when using an IDT, then the consideration of a vidicon tube, which will have an advantage only in sensitivity, is unnecessary.

The S/N (voltage) can be derived as follows:

$$S/N \cong \left(\frac{i_s}{2_e \Delta f}\right)^{1/2} \tag{7-1}$$

$$i_s = \frac{\pi N_\lambda \Delta\lambda q e T_o}{4 h\nu} \left(\frac{d_o \Delta l}{H}\right)^2 \tag{7-2}$$

$$f = \frac{V_r L N_s}{(\Delta l)^2} \tag{7-3}$$

where

i_s = output signal current
N_λ = nominal spectral radiance
$\Delta\lambda$ = spectral bandwidth
q = quantum efficiency (at λ)
e = electronic charge
T_o = optics transmission
d_o = optical aperture diameter
Δl = ground resolution element dimension (assumed square)
H = satellite altitude
$h\nu$ = photon energy (at λ)
Δf = electrical bandwidth
Vr = satellite relative velocity
L = ground swath width ($2H \tan \theta/2$)
N_s = number of separate spectral bands read out

Combining equations (7-1), (7-2), and (7-3) gives:

$$S/N = \frac{(\Delta l)^2 d_o}{2H} \left(\frac{\pi N_\lambda \Delta\lambda q \, To}{2 V_r L N_s h\nu} \right)^{1/2} \qquad (7\text{-}4)$$

To achieve the accuracy and precision given before it is required that

$$S/N \geq \frac{2N_\lambda}{\Delta N_\lambda} \qquad (7\text{-}5)$$

or

$$S/N \geq 33.3 \; (0.4 \rightarrow 0.5\mu)$$

and

$$S/N \geq 66.7 \; (0.5 \rightarrow 0.6\mu)$$

Therefore using the following equation (7-4) for $\lambda = 0.6\mu$, (worst case spectrally),

$S/N = 66.7$

$N_\lambda = 50 \text{ w/cm}^2/\mu/\text{ster} \; (4.64 \text{ w/m}^2/\mu/\text{ster})$

$\Delta\lambda = 0.02\mu$

$q = 0.07$ (Extended red S-20 or S-25 photocathode)

$T_o = 0.4$

$N_s = 15$

$h\nu = 3.31 \times 10^{-19}$ watts-sec

results in the relation:

$$\frac{(\Delta l)^2 d_o}{(H^3 V_r \tan \theta/2)^{1/2}} = 0.658 \times 10^{-5} \qquad (7\text{-}6)$$

Now the satellite ground speed, V_r, for a sun-synchronous orbit is only a function of the altitude, H. Also the period, P, to cover the earth is only a function of altitude. From the appropriate orbital tables, Figure 48 was constructed to show the relationship between P, θ, and H.

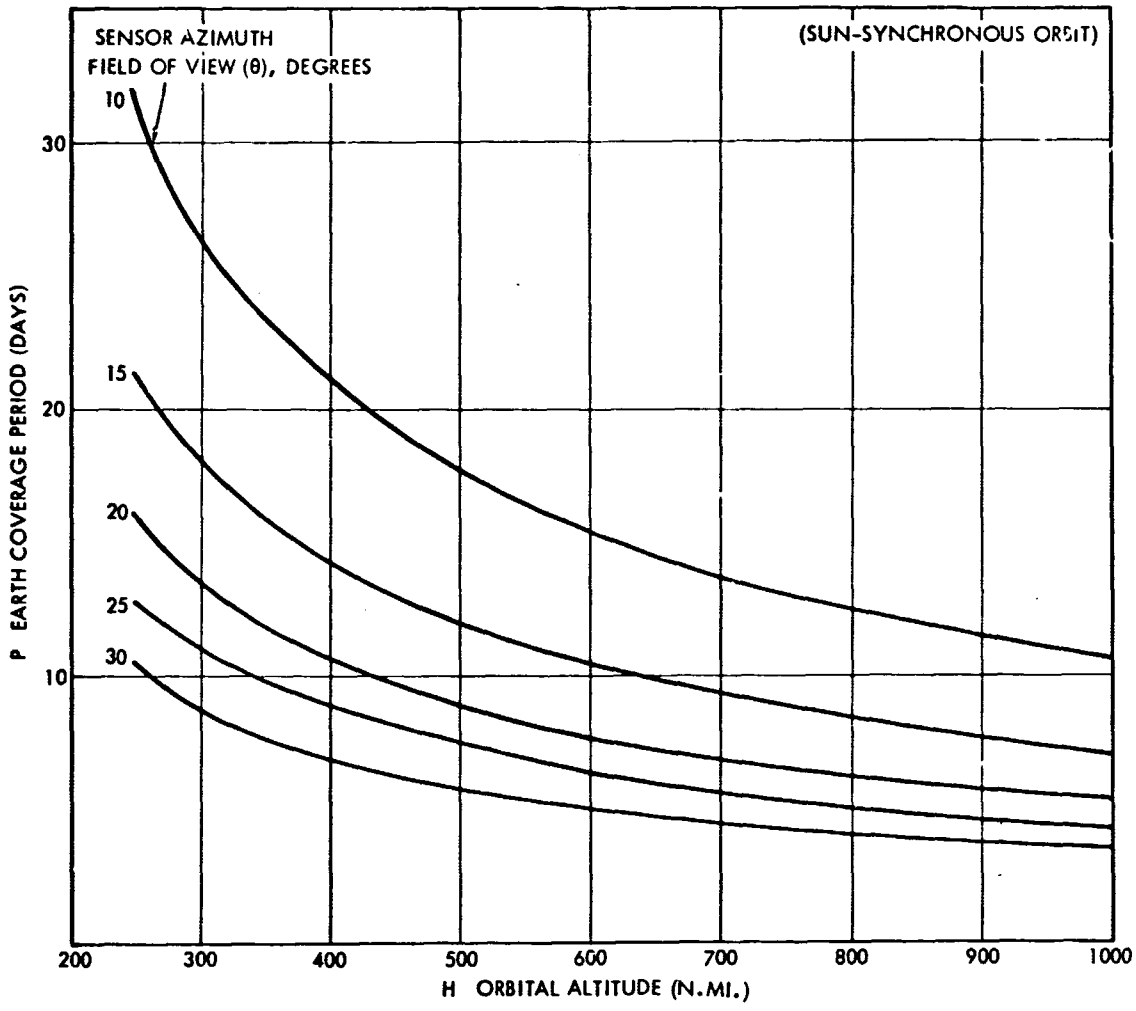

Figure 48. Tradeoff Between Sensor Field of View, Orbital Altitude and Earth Coverage Time

From Figure 48, four values of P (3.5, 7, 14, and 28 days) were chosen together with the appropriate values of θ and H. Using these values in equation (7-6) resulted in Table X, which gives the required minimum optical aperture diameter d_o at various ground resolution values. In addition the required number of resolution elements (N_l) is displayed. This comes from the relation:

$$N_l = \frac{2H \tan \theta/2}{\Delta l} \qquad (7\text{-}7)$$

Table X. Parameter Traueoff Between Ground Resolution, Period of Earth Coverage, Number of Resolution Elements and Objective Lens Diameter For Wisp, Ocean Color Sensor

Earth Coverage Period (Days)	From Figure 42 Azimuth		Number of Resolution Elements N_1 and Diameter of Objective Lens (inches)							
			Gnd. Res (ft) $\Delta 1$ = 1000		2000		4000		6000	
	Field of View (deg)	Altitude (n. mi)	N_1	d_o	N_1	d_o	N_1	d_o	N_1	d_o
3.5	30	1000	3260	232	1630	58	815	14.3	543	6.4
7	20	670	1432	49	716	12.6	358	3.1	2.39	1.4
7	30	392	1280	20	640	5.1	320	1.3	2.12	0.57
14	10	662	702	35	351	8.4	175	2.1	117	0.95
14	20	287	610	10.5	305	2.8	152	0.7	101	0.32
28	10	282	300	7.5	150	1.8	75	0.47	50	0.21

From the data of Table X, the remaining design parameters may be chosen. The values in the lower righthand portion of the table (separated by the heavy line) are considered to be feasible, essentially because values of d_o above 2 or 3 inches are difficult to instrument. Some IDT tubes are capable of up to 2000 lines, so except for one case, N_l is not the limiting factor.

The users of ocean color data have to ultimately decide on the desired earth coverage time, P. For the present a two week (14 day) period seems a reasonable design goal. Therefore the following design values were chosen:

P = 14 days
θ = 20 degrees
H = 287 nautical miles per hour
Δl = 2500 feet (square element)
d_o = 1.8 (minimum)
N_l = 244 resolution elements
θ = 20°

7.9 CHOICE OF COMPONENTS

In order to prove the feasibility of instrumenting these parameters, the availability of electro-optical components was investigated to meet these design goals. The wide angle image spectrophotometer (WISP) concepts* is to be considered as the system most feasible for this application.

The image tube chosen on the basis of size, ruggedization, and availability is the F4012 made by ITT. It has a usable photocathode of 0.70-inch diameter.

The conventional optical arrangement of the WISP system is shown in Figure 49. This arrangement has been used on some earlier prototypes and is used on the WISP IV, presently being flight-tested by TRW Systems.

*TRW Systems Patent Pending

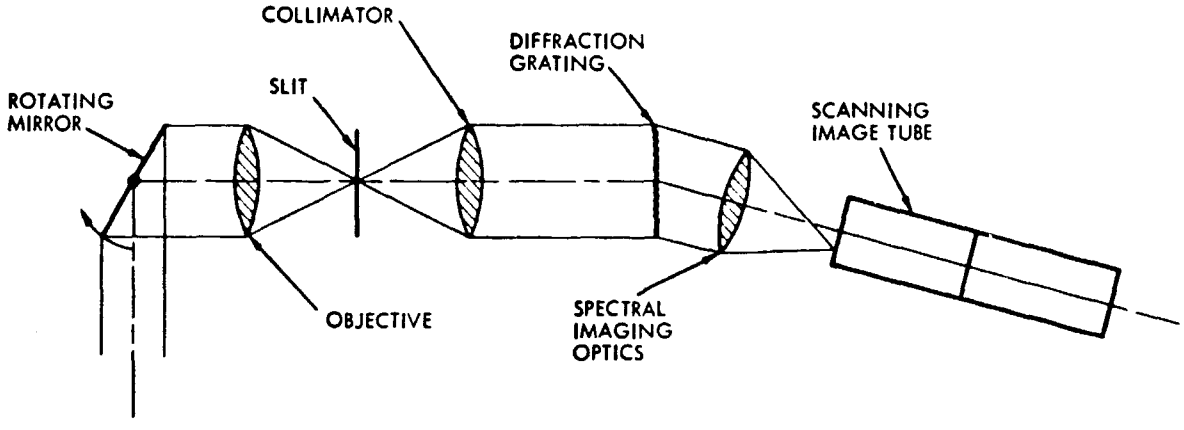

Figure 49. Conventional WISP Schematic

- The objective forms an image of the scene being viewed in the plane of the slit.
- Each element of the image falling on the slit is dispersed into a spectrum and the whole array of spectra (from all elements in the slit) is focused on the raster on the scanning image tube.
- The raster is scanned electronically and the distribution of intensity in each spectrum is sensed. In the time it takes to scan the whole raster the rotating mirror at the front of the device rotates just enough to move the image one slit width, thus placing a new series of spectra on the raster corresponding to a new set of image elements. The motion of the image across the slit can also be provided by the vehicle motion (as in an infrared scanner). The data are recorded or displayed.

Now if the objective and collimating lens are identical, vignetting occurs at the collimating lens for all images not on the optical axis. Therefore for a given relative aperture, (F/#), of the objective lens (determined by d_o, θ and the slit length), the F/# of the collecting lens has to be smaller (faster) to compensate for this vignetting loss.

In addition to this change in the conventional WISP design, another desirable feature is the use of only one lens to perform both the collimation and the spectral imaging. This requires the use of a reflection grating in a Littrow mounting, as depicted in Figure 50. A great advantage

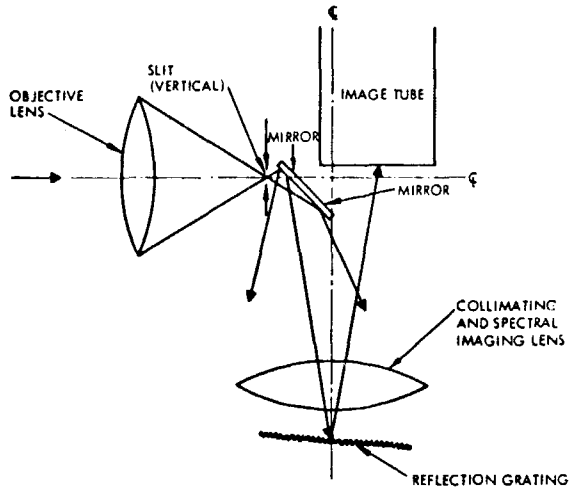

Figure 50. WISP Schematic for Ocean Color System

to this arrangement is that only two lenses instead of three require adjustment. With this arrangement some additional vignetting, although slight, will occur.

The slit length will be equal to 0.70 inch (the F4012 diameter) and for θ equal to 20 degrees, the focal length of the objective lens should equal 1.985 inches.

A readily available movie camera lens that will fit this requirement is the 50 mm, F/0.95 Angenieux Lens. Using this focal length (1.968 inches) requires a slight adjustment in some of the design parameters. Those affected are the following, which become

θ = 20.16 degrees

H = 287.6 nautical miles

N_L = 249 elements

d_o = 1.87 inches

Also,

L = 102.25 nautical miles

Δf = 34.4 kHz

The aperture available at the objective, 2.072 inches, will be used because it will help offset some of the vignetting, Also, using the same lens in front of the reflecting grating will result in a workable system. A detailed drawing of the electro-optical layout is shown in Figure 51. Some additional parameters needed to define the system are:

Grating Spacing = 8400 lines/inch (blazed grating, using 1st order.)

Grating angle = 5.3 degrees

Table XI sums up all of the system design parameters.

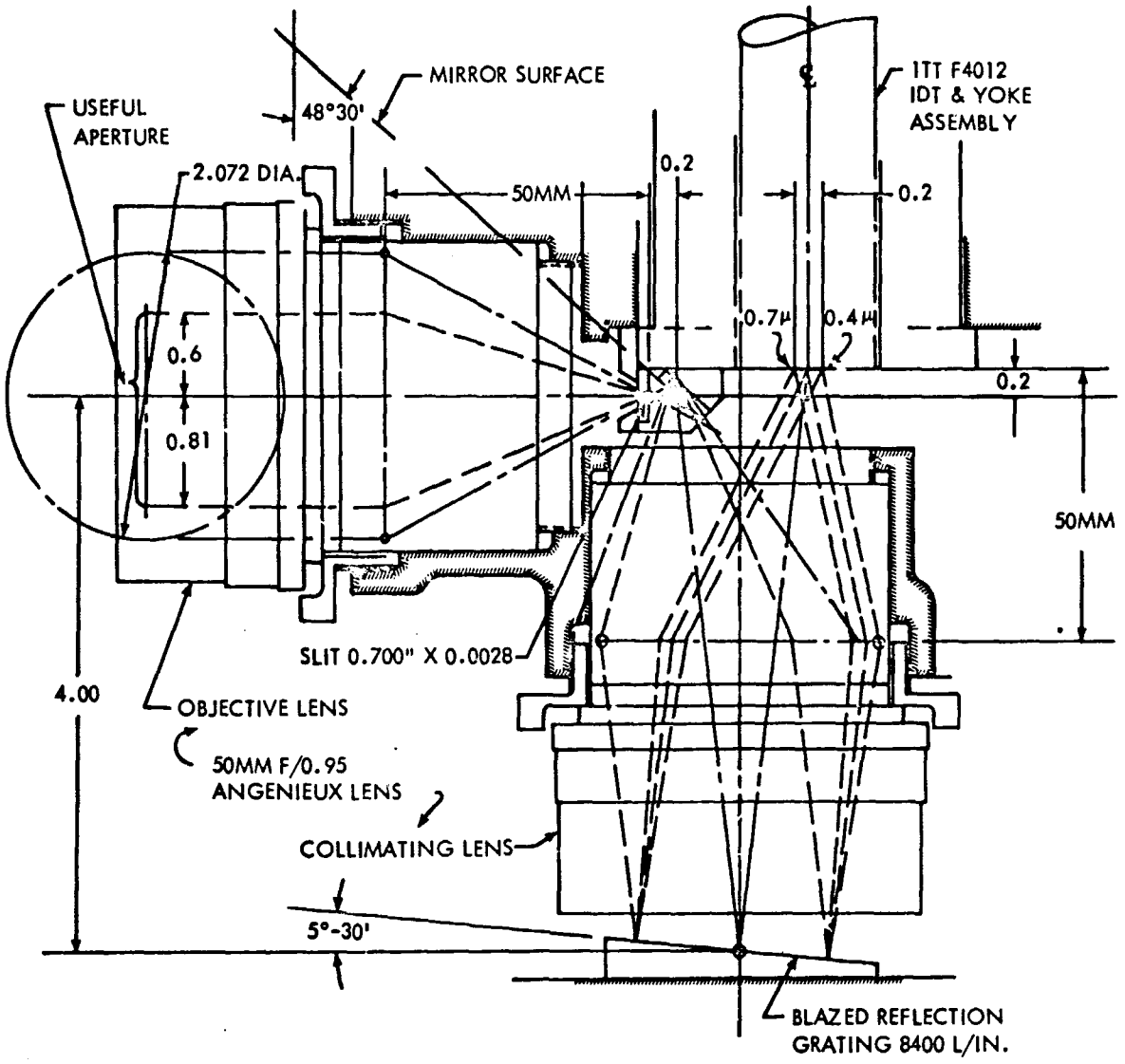

Figure 51. WISP Ocean Color Sensor Optical Layout

7.10 SYSTEM WEIGHT AND POWER

An estimate of the weight and power requirements of this WISP sensor indicates very moderate values for a satellite system. Table XII gives these estimates.

Table XI. Parameters of Ocean Color System

Item	Value	Units
1) Spectral Region	0.40 to 0.70	microns
2) Nominal Spectral Radiance (nadir)	50	$w/m^2/\mu/ster$
3) Maximum Spectral Radiance	300	$w/m^2/\mu/ster$
4) Measurement Accuracy		
(0.4 to 0.5 micron)	3.0	$w/m^2/ster/\mu$
(0.5 to 0.6 micron)	1.5	$w/m^2/ster/\mu$
5) Precision		
(0.4 to 0.5 micron)	1.5	$w/m^2/ster/\mu$
(0.5 to 0.6 micron)	0.75	$w/m^2/ster/\mu$
6) Spectral Resolution	0.02	microns
7) Number of Spectral Bands	15	———
8) Period for Complete Earth Coverage	14	days
9) Azimuth Field of View	20.16	degrees
10) Swath Width	102.25	n. mi.
11) Orbital Altitude	287.6	n. mi.
12) Resolution Element on Ground	2500	feet
13) Required Aperture Diameter (S/N = 66.7 at 0.6μ)	1.87	inches
14) Number of Spatial Resolution Elements	249	———
15) Electrical Bandwidth	34.4	kHz
16) Grating Spacing	8400	lines/inch
17) Grating Angle	5.3	degrees
18) Slit Length	0.700	inches
19) Slit Width	0.0028	inches

Table XII. WISP Weight and Power Requirements

Component	Weight (pounds)	Power (watts
IDT and Coil	2	1-2
Electronics	1	5
Optics	2	—
Structure	11	
Totals	16	6-7

7.11 SYSTEM FLIGHT TEST IN AIRCRAFT

It is feasible that this design for a satellite-borne ocean color system be first tested in an aircraft over selected portions of the oceans. It is interesting to note that V/H, the ground speed over the altitude, remains the same for a 250 ft/sec aircraft velocity flying at 17, 500 feet altitude. Therefore the bandwidth requirements and the expected S/N will be essentially equivalent to that expected at satellite altitude. The upward flux contributions from both the water and the atmosphere for the aircraft mounted sensor are greater than 50 percent of what would be realized at satellite altitude, with a hazy atmosphere (see Figure 44). For a clear atmosphere, the atmosphere contribution at 17, 500-feet altitude, is probably about 30 percent of that expected at satellite altitude, (see Figure 45). This is not too important, however, as the total amount from the atmosphere relative to that from the water is much less for the clear or Rayleigh case.

The main distinction between the 17, 500 feet and 300-nautical mile. altitudes is that the ground resolution element goes from 25 to 2500 feet. Thus flight test results from an aircraft may be more influenced by water surface phenomena (waves, whitecaps, etc), than would the satellite system where the resolution element of 2500 feet would integrate much of those effects.

7.12 ALTERNATIVE APPROACHES

Figure 38 shows clearly the change of the peak wavelength of the water reflectance curves as the amount of chlorophyll increases. Additional calculations of upward flux above the atmosphere were made to find

the value of wavelength where the peak occurs for both extremes of atmosphere. Figure 52 shows these results. A change in atmosphere does not appear critical in the value of peak wavelength.

If peak wavelength were accepted as the criteria of ocean productivity, the sensor design might be somewhat simplified. Only the wavelength region from about 0. 46 to 0. 55 micron would be of importance, as compared to a spectral region suggested before of three times this size.

The spectral resolution required would have to be somewhat smaller than 200 Å. A value of about 60 Å appears feasible from the curves. The main advantage, however, is that only relative measurements are required instead of absolute values and the precision of measurement (or S/N needed) is much less. This method is relatively insensitive to the presence of whitecaps, as the sunlight reflected from the whitecaps will be relatively unchanged over the wavelength region of interest.

The importance of this more simple approach can be investigated more thoroughly by analyzing the results of a flight test program of a device such as proposed above as the main approach to ocean color determination.

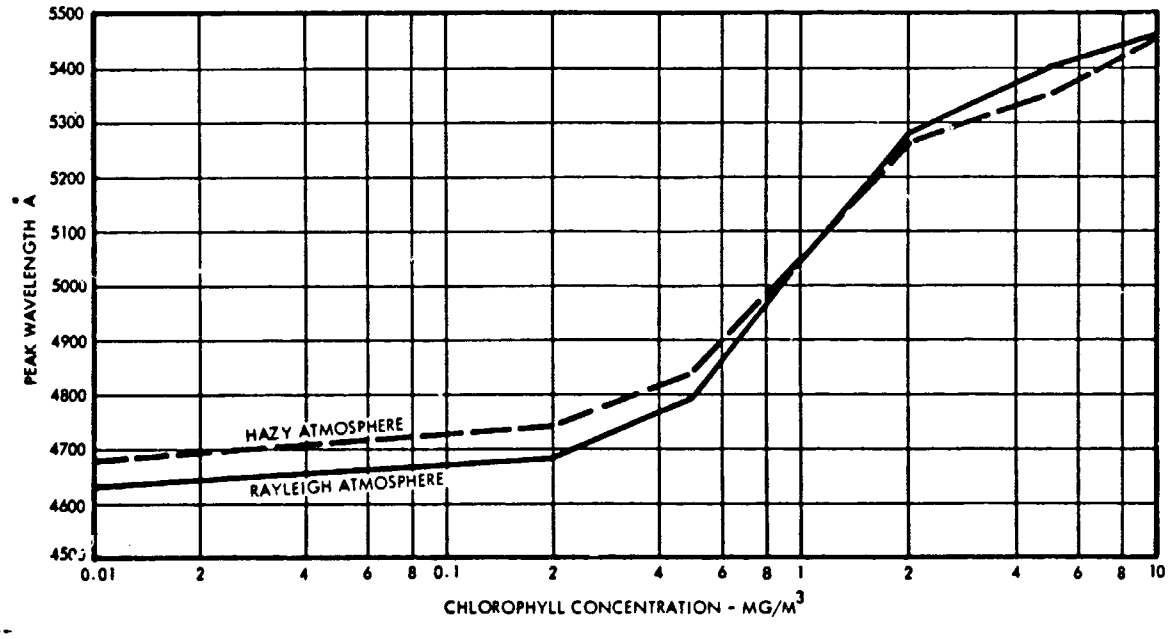

Figure 52. Wavelength Giving Peak Flux versus Chlorophyll Concentration

Finally, this alternative approach can be refined so that a very simple measurement is required. Consider the radiance centered around 0.470 μ and 0.540 μ with 0.03 μ bandpasses. If the measurements in these two bands are compared, moderately accurate determinations of chlorophyll content can be obtained at the higher concentrations. At lower concentrations the accuracy is not comparable to that obtained by the peak location method just described.

7.13 CORRECTION FOR SUN ANGLE, WATER SURFACE, AND ATMOSPHERE

In order to establish the "color" of a spatial resolution element of the ocean from the measured spectral radiance measured at the top of the atmosphere, it will be necessary to correlate these data with a standard set of curves, each corresponding to a range of chlorophyll content between 0 up to about 10 mg/m^3. These curves may be based on the calculations given here for various amounts of chlorophyll content, such as those of Figure 46, or more likely will be determined from empirical flight-test data and ground truth data. Variations, however, in sun angle, water surface, and atmosphere will affect the amount of upward flux measured, and must be accounted for before the correlation takes place.

7.13.1 Sun Angle Variations

From Figure 15, a 5σ value of maximum sea surface slope is about 0.120 or 10 degrees. Considering this value and the fact that the sensor will have a maximum view angle of 10 degrees in azimuth results in restricting measurements to solar zenith angles greater than about 30 degrees, if the specular reflection of the collimated radiation from the sun is to be excluded.

If the sun-synchronized orbit crosses the equator at an inclination of 96.6 degrees, the solar zenith angle when at the equator, is 35 degrees. When the satellite reaches 60 degrees latitude, north or south, the sun zenith will have increased to about 65 degrees and will have rotated 36 degrees in azimuth. If measurements are also restricted to values less than about 65 degrees, the total variation in solar irradiance on the ocean is minimal. Zenith angles greater than 65 degrees shift the spectral content of the sunlight far enough toward the red to move the spectral peaks.

These zenith angles (35 degrees and 65 degrees) correspond to values of m between about 1 and 2 (see Figures 1 and 2). The calculations performed in this study assumed a fixed sun angle of 45 degrees (m=1.4) and the actual solar spectral irradiance at the sea surface will vary from the conditions of calculation by about ±6 percent for a Rayleigh atmosphere or about ±10 percent for a turbid atmosphere. This variation (both in amplitude and in spectrum) can be easily taken into consideration in any correlation process.

7.13.2 Variation in Water Surface Reflection

A calm ocean reflects specularly the zenith skylight towards an observer at the zenith. As discussed earlier, the change in skylight intensity for increasing azimuth angles from the zenith is very small for those angles due to wave motion (see Figure 23). The spectral nature of the zenith skylight does change however, with aerosol content. Table XII lists the calculated contributions from each component of the upward flux reaching the top of the atmosphere, at these wavelength values, for both a clear (Rayleigh) atmosphere and a hazy atmosphere (Model D), for 0 and 5 mg/m^3 of chlorophyll.

The reflection from the surface is the smallest contribution, except at 0.7μ where the component from water with no chlorophyll is negligible. These data assume a smooth sea surface. It was apparent that a rough sea may double the surface reflection, presumably because of the introduction of white caps and the increase of albedo. The effect on the measured data would be an increase in amplitude only which would not have a major effect on the total upward flux but the spectral nature of the reflection should only be a function of the skylight itself. Consequently, even though it may be difficult to determine by an direct measurement from space the condition of the sea surface, the effect on the upward flux, particularly near the wavelength of maximum radiance, is not of great importance.

7.13.3 Changes in The Atmosphere

A variation in type of atmosphere can have a considerable influence on the ratio of atmospheric contribution to water contribution, as shown in Table XIII. Also, a comparison of Figures 44 and 45 show that a turbid atmosphere may contribute more than twice as much to the total upward

Table XIII. Contribution From Each Source To Upward Flux Measured Above Atmosphere For Two Atmosphere Extremes and Two Chlorophyll Contents

Atmosphere	Chlorophyll	Source	Wavelength — Å		
			4000	5500	7000
Clear	0	Water	46	14	0.7
		Surface	8	4	1.4
		Atmosphere	42	16	5.0
	5 mg/m^3	Water	15	62	11.0
		Surface	8	4	1.4
		Atmosphere	42	16	5.0
Hazy	0	Water	35	12	0.6
		Surface	6	6	4.0
		Atmosphere	91	50	19.0
	5 mg/m^3	Water	12	48	11.0
		Surface	6	6	4.0
		Atmosphere	91	50	19.0

Units - $\frac{W}{M^2 \mu}$

flux than would a clear atmosphere. Figure 47 shows the effect. The peak radiance (in π ster) at 0.46 micron varies from 172 to 130 $w/m^2/\mu$ as the atmosphere goes from very hazy to very clear. On the other hand, if it is assumed that the atmosphere remains turbid during a measurement, this decrease in peak radiance could correspond to a change in chlorophyll content from zero to about 0.5 mg/m^3. For an accuracy of measurement with this system of 0.2 mg/m^3, it would seem necessary to determine the turbidity (T) of the atmosphere to a value of plus or minus one. In other words, if T may vary between a value of one (Rayleigh) to a value of about five (most hazy condition), it should be necessary to categorize a particular atmosphere as having a turbidity factor T of either 1, 2, 3, 4, or 5 in order to correct the measured radiance and measure the chlorophyll content to the accuracy required.

7.13.4 Method of Atmosphere Correction

Two methods of atmosphere correction were discussed in Section 3.5. One (after the theory of Koschnieder) compares the brightness (or luminance) of an object of known reflectance against the brightness of the horizon. The main problem with this approach is that the object, or target of known reflectance, cannot be assumed to be always available. The second method, involving the measurement of the Stokes parameters of polarization, seems to hold the most promise for the future. The method requires much further development and it is felt that it is not within the scope of development of a satellite-borne, WISP-type system to incorporate this further complication. A possible parallel development program for this polarization device (whose success will provide much needed information to planetary investigators rather than oceanographers) is called for and it is understood to be underway.[17, 18, 19]

A third method, which would be simple to instrument, suggests itself. This involves a comparison of the radiance as measured from the nadir to that measured at some azimuth angle. Intuitively, there seems to be merit in this scheme. As the scattering path length of the atmosphere increases there is a greater contribution from the atmosphere and less from the water. As the atmosphere becomes more turbid, this effect should increase. The ratio of brightness at the nadir compared to that at some other angle, (assuming that the path lengths of both are through

homogeneous atmospheres and the ocean viewed in both fields of view is identical in composition) may show a predictable difference as a function of atmospheric turbidity.

In order to quantitatively evaluate this method of correction, equations were derived for the radiation measured directly downward to the light measured at an angle for each of the three components. These equations can then be used in an overall equation which will give the water contribution by itself, provided the assumption is made that the contribution from the surface is a constant such as 10 percent of the total upward flux.

The following relationship relates the radiation from the water (subsurface only) measured at the nadir, E_{w_o}, with that measured at an angle, α, denoted by E_w.

$$\frac{E_w}{E_{w_o}} = \frac{1-e^{-\sigma_{\theta,\alpha}\left(\frac{H}{\cos\alpha}\right)}}{1-e^{-\sigma_\theta H}} \left(\frac{1-R}{1-R_o}\right)_\alpha \left(\frac{T}{T_o}\right)_\alpha$$

where σ is the scattering coefficient, R is the reflectivity, θ is sun angle and T is transmission. For all practical cases, this reduces to

$$\frac{E_w}{E_{w_o}} = \frac{\sigma_{\theta,\alpha}}{\sigma_\theta \cos\alpha} \left(\frac{1-R}{1-R_o}\right)_\alpha \left(\frac{T}{T_o}\right)_\alpha \quad (\text{for } \sigma \geq 0.2)$$

The probable error in evaluating these terms is:

$\frac{\sigma_{\theta,\alpha}}{\sigma_\theta}$ 50 percent

$\left(\frac{1-R}{1-R_o}\right)_\alpha$ 1 percent

$\left(\frac{T}{T_o}\right)_\alpha$ 5 percent

These error are evaluated as follows.

The error in scattering coefficient ratio is due to the fact that there is no a priori knowledge of particles in the water whose content strongly affects the amount and direction of scattering. It might be possible by iterative techniques to reduce this substantial error somewhat. The error in the reflection coefficient term is very small because of knowledge of the Fresnel relationship. The error in the atmospheric transmissivity term is due to variations in weather over the path measured at an angle.

The following equation is the relationship for the ratio of radiation reflected from the surface, for the nadir and the angle, α:

$$\frac{E_\alpha}{E_o} = \left(\frac{R}{R_o}\right)_\alpha \left(\frac{L}{L_z}\right)_{\alpha,\theta} \left(\frac{T}{T_o}\right)_\alpha$$

where L_z is the skylight brightness at the zenith, and L is the value of brightness for that portion of the sky which is reflected at angle α.

Each of those three terms can be calculated from a knowledge of view angle α and sun angle θ. The probable errors are:

$\left(\frac{R}{R_o}\right)_\alpha$ 1 percent

$\left(\frac{L}{L_z}\right)_{\alpha,\theta}$ 5 percent

$\left(\frac{T}{T_o}\right)_\alpha$ 5 percent

The error in the sky brightness term is assumed small because of the data of Figure 11. The other two terms are taken as before.

Finally, the relationship for the scattered airlight is

$$\frac{E_A}{E_{A_o}} = \frac{1-e^{-\sigma_{\theta,\alpha}\frac{H}{\cos\alpha}}}{1-e^{-\sigma_\theta H}}$$

where now σ refers to the atmospheric scattering, and for moderate scattering,

$$\frac{E_A}{E_{A_o}} = \frac{\sigma_{\theta,\alpha}}{\sigma_\theta \cos\alpha}$$

The probable error in evaluating the term,

$$\frac{\sigma_{\theta,\alpha}}{\sigma_\theta}$$

is taken as 15 percent.

Combining the probable errors just discussed, in a manner to evaluate the probable error in determining the water contribution by itself, results in errors of over 100 percent even with the case where the water scattering coefficient ratio error (taken as 50 percent above) is zero.

It is concluded, therefore, that this approach is not too promising, although in a flight-test program of the WISP sensor, these measurements can be easily made and an empirical evaluation of this technique can be easily obtained.

8. CONCLUSIONS

On the basis of this study, the following ideas seem of greatest importance:

1. Calculations indicate definite changes in the spectral nature of the upward flux from the ocean as the chlorophyll content is varied. Also, the wavelength of peak of upward flux appears to correlate with chlorphyll concentration.

2. Since these calculations are based on assumed ocean characteristics with chlorophyll only as the variable, empirical data are needed to modify these calculated curves. Before a standard set of spectral radiance curves versus chlorophyll content can be used to denote the real oceans, the influence (although of possibly secondary importance) of other ocean constituents such as "yellow matter" and particulates must be measured.

3. To achieve an accuracy of 0.2 mg/m^3 for the chlorophyll content in the ocean, the turbidity of the atmosphere must be determined to within 20 percent.

4. A simple WISP system of moderate values of aperture and electrical bandwidth, in conjunction with an available image dissector tube, will meet all the necessary system specifications required to measure the radiance from the ocean.

5. A prototype of this system can be flown in an aircraft and simulate the actual performance at satellite altitude. This is because V/H can be made the same and most of the atmosphere is below this altitude.

6. An adequate method needs to be developed to independently measure the optical density of the atmosphere. The measurement of the Stokes parameters seems to hold the best promise for the future. A comparison of the radiance from the nadir and that from some azimuth angle of view is attractive because of its simplicity; however, an estimate of the uncertainties involved makes this approach questionable. During an aircraft flight test of the WISP system this latter method could be easily tried.

9. REFERENCES

1. Kondrat'yev, K. Y., Actinometry, Translation of "Aktinometriza Gidrometeorologicheskoye dzdatel'stvo," Leningrad, 1965, NASA TT F-9712, November 1965.

2. Johnson, Francis S., "The Solar Constant," Journal of Meteorology, Volume 11, No. 6, pp 431-439, December 1954.

3. Moon, Parry, "Proposed Standard Solar-Radiation Curves for Engineering Use," Journal of Franklin Institute, Volume 30, pp 583-619, 1940.

4. Elterman, L., "Atmospheric Attenuation Model, 1964, in the Ultraviolet, Visible, and Infrared Regions for Altitudes to 50 km," AFCRL Environmental Research Paper No. 46, L. G. Hanscom Field, Massachusetts, 1964.

5. Curcio, J. A. and Knestrick, G. L., "An Atlas of the Absorption of the Atmosphere from 5400 to 8520A," NRL Report 4601, August 1955.

6. Kondrat'yev, K. Y., Andreev, J. D., Badinov, I. Y., Grishechkin, V. S., and Popova, L. V., "Atmospheric Optics Investigations on Mt. Elbrus," Applied Optics, Volume 4, No. 9, pp 1069-1076, September 1965.

7. Junge, Christian E., "Atmospheric Chemistry," Advance in Geophysics Vol. 4, pp 1 - 108, 1958.

8. Middleton, W. E. K., "Vision through the Atmosphere," University of Toronto Press, Toronto, Canada, 1952.

9. Roll, H. V., Physics of the Marine Atmosphere, Academic Press, New York and London, 1965.

10. Junge, C. E. and Manson, J. E., "Stratospheric Aerosol Studies," Journal of Geophysical Research, Volume 66, pp 2163 - 2182, July 1961.

11. Kondrat'yev, K. Y., Nicolsky, G. A., Badinov, I. Y., and Andriev, S. D., "Direct Solar Radiation up to 30 km and Stratification of Attenuation Components in the Stratosphere," Applied Optics, Volume 6, No. 2, pp 197-207, February 1967.

12. Lloyd, J. W. F., Silverman, S., Nardone, L. S. and Cochrun, B. L., "Day Skylight Intensity from 20 km to 90 km, at 5500Å," Applied Optics, Volume 4, No. 12, pp 1602 - 1606, December 1965.

13. Curcio, J. A. and Durbin, K. A., "Atmospheric Transmission in the Visible Region," NRL Report 5368, October 1959.

REFERENCES (Continued)

14. Curcio, J. A., Knestrick, G. L., and Corden, T. H., "Atmospheric Scattering in the Visible and Infrared," NRL Report 5567, January 1961.

15. Koschmieder, H., Beitr, Phys. freien Atmosph., Volume 12, No. 33 pp 171, 1924.

16. Duntley, Seibeit Q., "The Reduction of Apparent Contrast by the Atmosphere," Journal of the Optical Society of America, Volume 38, No. 2, pp 179 - 191, February 1948.

17. Rao, C. R. Nagaraja and Sekera, Z., "A Research Program Aimed at High Altitude Balloon-Borne Measurements of Radiation Emerging from the Earth's Atmosphere," Applied Optics, Volume 6, No. 2, pp 221-225, February 1967.

18. Sekera, Z., "Determination of Atmospheric Parameters from Measurement of Polarization of Upward Radiation by Satellite or Space Probe," ICARUS, Volume 6, pp 348 - 359, May 1967.

19. Sekera, Z., Rao, C. R. Nagaraja, and Dibble, D., "Photoelectric Skylight Polarimeter," The Review of Scientific Instruments, Volume 34, No. 7, pp 764-768, July 1963.

20. Taylor, A. H. and Kerr, G. P., "The Distribution of Energy in the Visible Spectrum of Daylight," Journal of the Optical Society of America, Volume 31, pp 3 - 8, January 1941.

21. Dorno, C., "Himmelshelligkeit, Himmelspolarisation and Sonnenintensität in Davos 1911 bis 1918," Veröffentle Preuss. Meteorol. Inst. Abhandl., 8, No. 303, 1919.

22. Boileau, Almerian R., "Atmospheric Properties," Applied Optics, Volume 3, No. 5, pp 570 - 581, May 1964.

23. Powell, Wilson M. and Clarke, George L., "The Reflection and Absorption of Daylight at the Surface of the Ocean," Journal of the Optical Society of America, Volume 26, pp 111 - 120, March 1936.

24. Cox, Charles, and Munk, Walter, "Measurement of the Roughness of the Sea Surface from Photographs of the Sun's Glitter," Journal of the Optical Society of America, Volume 44, No. 11, pp 838 - 850, November 1954.

25. Stamm, Gordon L. and Langel, Robert A., "Some Spectral Irradiance Measurements of Upwelling Natural Light off the East Coast of the United States," Journal of the Optical Society of America, Volume 51, No. 10, pp 1090 - 1094, October 1961.

REFERENCES (Continued)

26. Duntley, Seibert Q., "Light in the Sea," Journal of the Optical Society of America, Volume 53, pp 214 - 233, February 1963.

27. Hulburt, E. O., "Propagation of Radiation in a Scattering and Absorbing Medium," Journal of the Optical Society of America, Volume 33, pp 42 - 45, January 1943.

28. Hulburt, E. O., "Optics of Distilled and Natural Water," Journal of the Optical Society of America, Volume 35, No. 11, pp 698 - 705, November 1945.

29. Jerlov, Nils G., "Optical Studies of Ocean Waters," Reports of the Swedish Deep-Sea Expedition, Volume III, Physics and Chemistry, No. 1, 1948.

30. Kallem, K., "Zum Problem der Meereswasserfarbe," Ann. d. Hydr. usw., Volume 66, H. 1, pp 1 - 13, 1938.

31. Clarke, George L. and James, Harry R., "Laboratory Analysis of the Selective Absorption of Light by Sea Water," Journal of the Optical Society of America, Volume 29, pp 43 - 55, February 1939.

32. Smith, Raymond C., and Tyler, John E., "Optical Properties of Clear Natural Water," Journal of the Optical Society of America, Volume 57, No. 5, pp 589 - 595, May 1967.

33. Dawson, L. H., and Hulburt, E. O., "Angular Distribution of Light Scattered in Liquids," Journal of the Optical Society of America, Volume 31, pp 554 - 558, August 1941.

34. Jerlov, Nils G., "Optical Classification of Ocean Water," Symposium on the Physical Aspects of Light in the Sea, John E. Tyler, Editor, University of Hawaii Press, Honolulu, Hawaii, pp 45 - 49, 1964.

35. Ivanoff, Alexander, "Measurement at Sea of Water Samples," Symposium on the Physical Aspects of Light in the Sea, John E. Tyler, Editor, University of Hawaii Press, Honolulu, Hawaii, pp 11 - 17, 1964.

36. Yentsch, Charles S., "The Influence of Phytoplankton Pigments on the Colour of Sea Water," Deep-Sea Res., Volume 7, pp 1 - 9, 1960.

37. Yentsch, Charles S., "Measurement of Visible Light Absorption of Particulate Matter in the Ocean," Deep-Sea Res., Volume 6, pp 207 - 217, 1962.

38. Tyler, John E., "In Situ Detection and Estimation of Chlorophyll and other Pigments – Preliminary Results," Botany, Volume 51, pp 671 - 678, 1964.

REFERENCES (Concluded)

39. Holmes, R. W., "Surface Chlorophyll 'A', Surface Primary Production, and Zooplankton Volumes in the Eastern Pacific Ocean," Rapp et Proc. - Verb., Cons. Internat. Explor. de la Mer., Volume 144, pp 109 - 116, 1958.

40. Blackburn, Maurice, "Relationships between Standing Crops at Three Successive Tropic Levels in the Eastern Tropical Pacific," Pacific Science, Volume 20, pp 36 - 59, January 1966.

41. Tyler, J. E. and Smith, R. C., "Spectroradiometric Characteristic of Natural Light Under Water," Journal of the Optical Society of America, Volume 57, No. 5, pp 595 - 601, May 1967.

42. Fraser, Robert S., "Computed Intensity of Polarization of Light Scattered Outwork from the Earth and an Overlying Aerosol," Journal of the Optical Society of America, Volume 54, No. 2, pp 157 - 168, February 1964.

43. Fraser, Robert S., (Private Communication).

44. Elterman, L. "A Model of a Clear Standard Atmosphere for Attenuation in the Visible Region and Infrared Windows," AFCRL Report 63-675, July 1963.

45. Deirmendjian, Diran and Sekera, Zdenek, "Global Radiation Resulting from Multiple Scattering in a Rayleigh Atmosphere," Tellus, Volume VI, No. 4, pp 383 - 398, 1954.

46. Perrin de Brichambaut, C., "Rayonnement Solaire et Ezhanges Radiatifs Naturlis Gauthier-Villars," Paris, 1963.

APPENDIX A

CALCULATIONS OF UPWARD FLUX FROM OCEAN USING EQUATIONS OF HULBURT

Hulburt[20] derived a general expression for the light coming out of the sea in terms of the optical constants of the sea water. Later, Hulbert[21] added a surface reflection term to these equations. The general expression, (for deep water and therefore no bottom reflection), is

$$b_o = a_o [(1 - r_c)(1 - r_d)\gamma + r_c] + i_o (1 - r_c)^2 \gamma' \qquad \text{(A-1)}$$

with

$$\gamma = (1 - \eta_d)\sigma_d [\beta_d + (1 - \eta_d)\sigma_d + \gamma]^{-1} , \qquad \text{(A-2)}$$

$$\gamma' = [(1 - \eta_c)\sigma_c - D \cos \zeta (\gamma - A)] [\beta_d + (1 - \eta_d)\sigma_d + \gamma]^{-1} , \qquad \text{(A-3)}$$

$$\gamma = \left| \beta_d [2 (1 - \eta_d)\sigma_d + \beta_d] \right| 1/2 \qquad \text{(A-4)}$$

$$A = (\beta_c + \sigma_c) \sec \zeta \qquad \text{(A-5)}$$

and

$$D = \sigma_c [(1 - \eta_c)(\beta_d \cos \zeta - \beta_c - \sigma_c) + (1 - \eta_d)\sigma_d \cos \zeta]$$

$$X[(\beta_c + \sigma_c)^2 - \gamma^2 \cos^2 \zeta]^{-1} \qquad \text{(A-6)}$$

A definition of the various terms follows:

- b_o is the total upward flux emerging from the ocean, outside of the specularly reflected solar energy. and includes both the backscattered radiation and the reflected skylight.
- a_o is the skylight irradiance on the surface.
- i_o is the collimated irradiance from the sun reaching the surface.
- r_d is the surface reflectance for diffuse radiation.
- r_c is the surface reflectance for collimated radiation.

σ_d is the scattering coefficient of the water for diffuse radiation.

σ_c is the scattering coefficient of the water for collimated radiation.

β_d is the absorption coefficient of the water for diffuse radiation.

β_c is the absorption coefficient of the water for collimated radiation.

$\eta_c \sigma_c$ is the fraction of the collimated radiation scattered in the forward direction; $(1 - \eta_c)\ \sigma_c$ is scattered backward.

$\eta_d \sigma_d$ is the fraction of the diffuse radiation scattered in forward direction; $(1 - \eta_c)\ \sigma_d$ is scattered backward.

ζ is the solar zenith angle.

Calculations of b_o were performed, using the above equations, by assuming various values of the absorption coefficient, β, (corresponding to varying amounts of chlorophyll) over the spectral region from 0.400 to 0.700 micron. In addition, the scattering coefficients, σ, were assumed to vary from a selective value (Rayleigh) for clear waters to the non-selective value (Mie) for the high chlorophyll concentrations. The following values were used:

ζ = 45 degrees

r_d = 0.066 (from Hulburt [28])

r_c = 0.052 (calculated from Fresnel Equation for ζ = 45 degrees, and assumed constant with wavelength. A calm sea is also assumed.)

$\left.\begin{aligned} \beta_d &= 2\beta_c \\ \sigma_c &= 2\sigma_c \end{aligned}\right\}$ (from Hulburt [28])

β_c is taken from Yentsch[36], who measured the absorption of chlorophyll. Figure A-1 is a plot of the combined spectral absorption coefficient of water and chlorophyll. Some measured data from the laboratory for two waters are also shown. σ_c is assumed to vary as shown in Figure A-2. The values used by Hulburt[28], in his calculations for distilled water and Chesapeake Bay water, were assumed to correspond to the chlorophyll contents of 0.0 and 10.0 mg/m^3. Between 0.0 and 10.0 the end points were taken as linearly dependent on the amount of chlorophyll, with straight lines used to connect these end points on the log-log

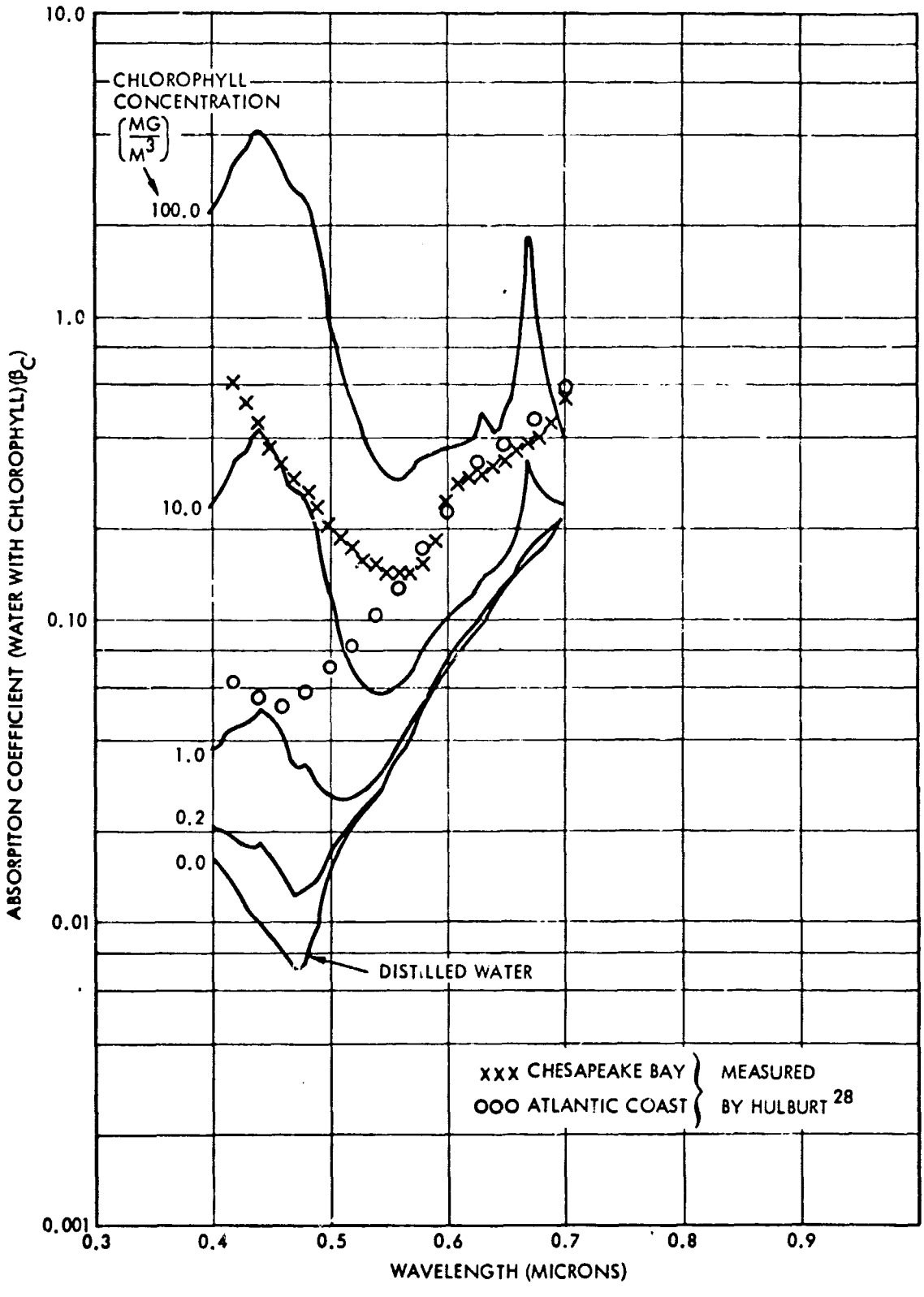

Figure A-1. Combined Absorption Coefficients for Pure Water and Plant Pigments, Over the Range of 0 to 100 mg/m^3 of Chlorophyll, Yentsch[36]

g/m^3, the nonselective character of the data
value directly proportional to the quantity of

linearly between 0.864 for distilled water (from
mg/m^3 (measured by Hulburt[21] for Chesapeake
equal to η_d. From 10 to 100 mg/m^3, the value
ain constant.

heric conditions were assumed which affect the
st case is that of a very turbid atmosphere,
ctor of 4.5. [A Rayleigh atmosphere, (con-
as a value of turbidity equal to 1.0; the
zenith direction at about 0.6μ is a factor 4.5
leigh atmosphere]. The second case assumes
and thus the spectral nature of i_o and a_o for
racket all possible atmospheric conditions to
ss, sunny day. The values of i_o and a_o were
of Diermendijizn and Sekera[45], who give the
lar and sky radiation on the surface for a

ken from Figure 2 for m = 1.4 (ξ= 45°). The
from Kondrat'yev[1] (page 326) who gives
y radiation as shown in Figure A-3. The
d by assuming that the integrated solar
and 0.7μ, if i_o is 7 times that from the sky,
ed by Hulburt[28], as shown in Table VII for a
ions on the data of Deirmendjian and Sekera[45]
the Rayleigh atmosphere. Perrin de
[46] generally the solar radiation is approximately
al value. For the more turbid atmosphere the
s greater. Figure A-4 gives the spectral
of i_o and a_o.

he variation in the spectral nature of the sky
data are given in Figure 10 from Taylor and
the range of clear sky to that of a smoky and
ky. The spectral distribution used above for

the sky for a Rayleigh atmosphere is very similar to that of curve A of Figure 10. The spectral nature of the turbid atmosphere (T = 4. 5) used above is similar to that of curve D but has slightly less relative blue radiation.

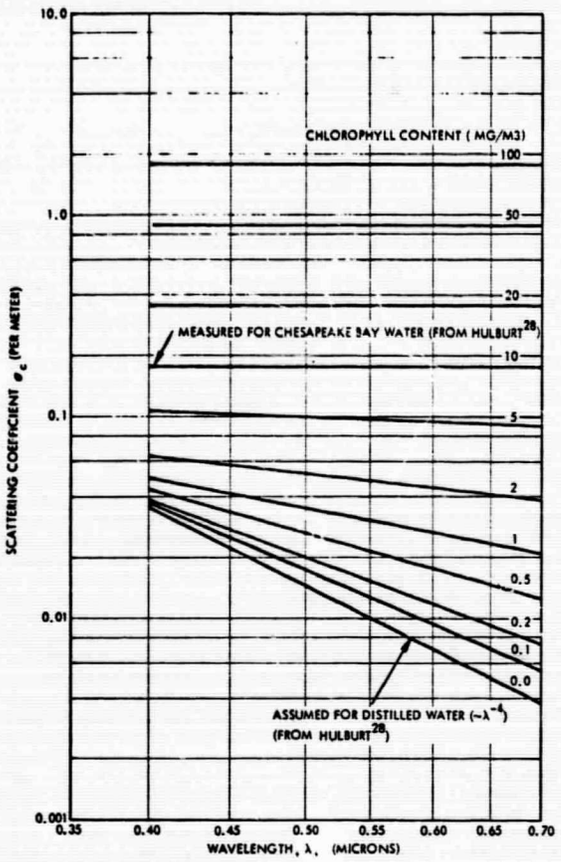

Figure A-2. Assumed Spectral Scattering Coefficients for Water with Varying Amounts of Chloropnyll

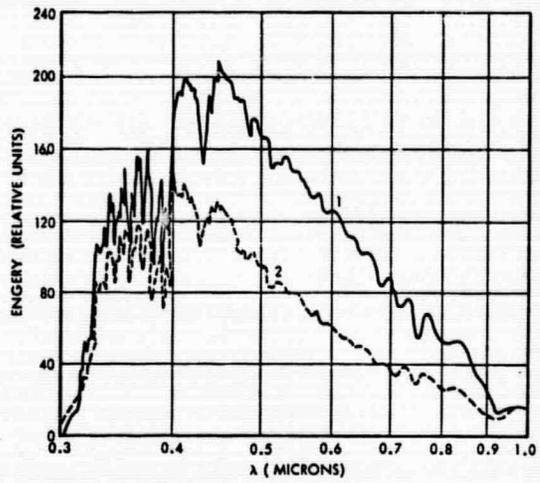

Figure A-3. Spectral Distribution of Scattered Radiation in a Cloudless Sky at the Zenith (1) and at a Point Where Sky Brightness is Minimal (2). (Solar Zenith Angle is 45°; T = 4.5), Kondrat'yev[1]

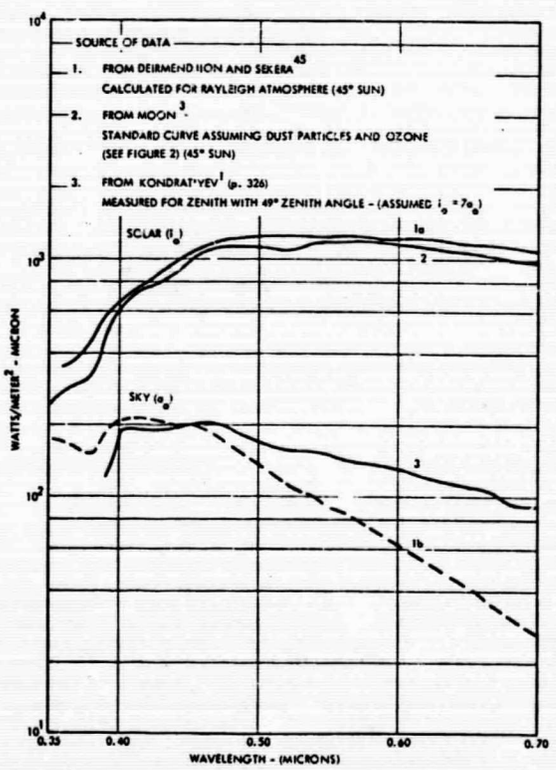

Figure A-4. Spectral Irradiance from Sun (i_o) and Sky (a_o) for Turbid and Rayleigh Atmospheres